Knockout of the glutamate transporter GLT-1 specifically from neurons drastically alters transcriptome profiles in CA3, CA1, and Striatum

by

Alexander Cory Wright Houston

B.S. Neuroscience
Indiana University, 2011

Submitted to the Department of Brain and Cognitive Sciences in Partial Fulfillment of the Requirements for the Degree of

Master of Science in Brain and Cognitive Sciences
at the
Massachusetts Institute of Technology

September 2015

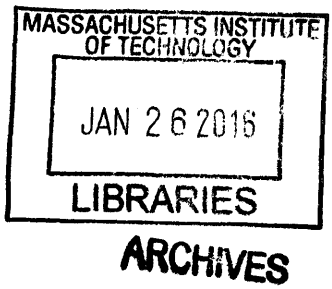

Signature of Author: Signature redacted
Department of Brain and Cognitive Sciences
August 7, 2015

Certified by: Signature redacted
Matthew A. Wilson
Sherman Fairchild Professor of Neuroscience
Thesis Supervisor

Accepted by: Signature redacted
Matthew A. Wilson
Sherman Fairchild Professor of Neuroscience
Director of Graduate Education for Brain and Cognitive Sciences

Knockout of the glutamate transporter GLT-1 specifically from neurons drastically alters transcriptome profiles in CA3, CA1, and Striatum

by

Alexander Cory Wright Houston

Submitted to the Department of Brain and Cognitive Sciences
on August 7, 2015 in Partial Fulfillment of the Requirements
for the Degree of Master of Science in
Brain and Cognitive Sciences

Abstract

Precise regulation of glutamate homeostasis is critical for normal brain function, as its disruption can impair excitatory transmission and result in neuro-degenerative and neuropsychiatric disorders. Critical to maintaining glutamate homeostasis is a family of sodium-dependent glutamate transporters. GLT-1, the major glutamate transporter, is responsible for >90% of brain glutamate uptake. While previously thought to exist solely on astrocytes, the Rosenberg lab has identified GLT-1 as the major, if not only, glutamate transporter associated with excitatory terminals, particularly in CA3 pyramidal neuron axon terminals within CA3 and CA1 as well as in cortical layer V pyramidal neuron axon terminals within striatum. The specific functions of GLT-1 in axon terminals in regulating glutamate homeostasis and synaptic transmission are unknown; in order to investigate these functions, the Rosenberg lab has generated a conditional GLT-1 KO mouse line where GLT-1 can be specifically deleted from neurons.

The aim of this project was to investigate the transcriptome profiles resultant from knockout of neuronal GLT-1 (nGLT-1), within regions known to express GLT-1 on neurons, and to identify and characterize alterations in known biological pathways. I report that deletion of nGLT-1 results in a high degree of differential gene expression within CA3 (1509), CA1 (322), and Striatum (1268). Furthermore, these alterations in gene expression were enriched in annotated biological pathways related to energy metabolism and neurotransmission. These findings challenge the long-held assumption that, because GLT-1 expression on neurons is significantly lower than on astrocytes, nGLT-1 contributes little to the regulation of synaptic glutamate homeostasis.

Thesis Supervisor: Matthew A. Wilson

Title: Sherman Fairchild Professor of Neuroscience

To Katy and Noel, for all of your support.

Table of Contents

Chapter 1: Introduction 5
- Glutamate 5
- Regulation of glutamate homeostasis 5
- The importance of GLT-1 7
- Neuronal GLT-1 7
- Neuronal specific deletion of GLT-1 8
- Aim 10

Chapter 2: Materials and Methods 11
- Subjects 11
- Tissue preparation 11
- RNA isolation 12
- RNA sequencing library construction 13
- RNA sequencing 20
- RNA sequencing analysis pipeline 21
- Pathway analysis 25
- Statistics 26

Chapter 3: Results 27
- CA3 27
- CA1 29
- Striatum 30

Chapter 4: Discussion 33
- Overview of main findings 33
- Oxidative phosphorylation 33
- Calcium signaling and neuroactive ligand-receptor interaction 35
- Disruption in specific neurotransmitter systems within striatum 37
- Conclusions 38

Chapter 5: Figures 40
- CA3 40
- CA1 47
- Striatum 53

Chapter 6: References 66

Chapter 1

Introduction

Glutamate

Glutamate is a proteinogenic amino acid and is the primary excitatory neurotransmitter in the brain (Danbolt, 2001). Glutamate functions as a neurotransmitter by activating its cognate receptors, which include three classes of ionotropic (NMDA, AMPA, Kainate) and several subtypes of metabotropic (mGlu) receptors, and is essential for normal brain function and development (Fonnum, 1984; Hack and Balázs, 1994; Yano et al., 1998; Danbolt, 2001; Dong et al., 2009). However, glutamate is also neurotoxic; prolonged exposure to glutamate in the extracellular space can result in cellular damage via excessive Ca^{2+} influx through over-activation of receptors, termed excitotoxicity (Dong et al., 2009). Therefore, precise regulation of glutamate levels is essential, as its disruption can impair excitatory transmission (Danbolt, 2001) and result in various disease states (Blandini et al., 1996; Goff and Coyle, 2001; Goursaud et al., 2008; Lisman et al., 2008; Miller et al., 2008; Zink et al., 2010; Fischer et al., 2013; Paula-Lima et al., 2013).

Regulation of glutamate homeostasis

Glutamate homeostasis involves the regulation of glutamate levels in the extracellular synaptic and extra-synaptic environments. It affects synaptic activity and plasticity by controlling glutamate access to its ionotropic and metabotropic

receptors. A crucial factor in maintaining glutamate homeostasis is the balance between synaptic and glial glutamate release and elimination. For synaptic release, glutamate is transported into synaptic vesicles by vesicular glutamate transporters and subsequently released by a Ca^{2+} dependent exocytotic process (Cousin and Robinson, 1999). Glutamate can also be released extra-synaptically by astrocytes; the cysteine-glutamate exchanger xCT, which exchanges one extracellular cystine molecule for one intracellular glutamate molecule (McBean, 2002), accounts for the majority of extra-synaptic extracellular glutamate (Baker et al., 2002). Furthermore, glutamate receptors are found on most cellular processes (i.e., dendrites, cell bodies, nerve terminals). In order to avoid excitotoxic-related events, glutamate must be rapidly removed from the extracellular space. There has yet to be an enzyme identified in the extracellular space to metabolize glutamate and, thus, the only means of removing glutamate from this area is via its uptake (Balcar and Johnston, 1972; Logan and Snyder, 1972; Takahashi et al., 1997; Danbolt, 2001).

The only known mechanism for glutamate clearance is provided by five excitatory amino acid transporters (EAAT1-5); the corresponding rodent analogs of the human EAATs are GLAST, GLT-1, EAAC1, EAAT4, EAAT5, respectively (Danbolt, 2001). GLT-1 and GLAST are expressed throughout the brain, primarily in the plasma membrane of glial cells. EAAC1 and EAAT4 are expressed post-synaptically in the plasma membranes of dendritic spines, with EAAT4 being expressed only in cerebellar Purkinje cells and EAAC1 throughout the brain. EAAT5 is expressed in neurons throughout the retina.

The importance of GLT-1

Of the five glutamate transporters, GLT-1 is the most abundantly expressed, representing ~1% of total brain protein (Lehre and Danbolt, 1998), and is responsible for >90% of brain glutamate uptake (Tanaka et al., 1997; Danbolt, 2001). GLT-1 is the only glutamate transporter whose knockout is lethal (Tanaka et al., 1997) and its deletion knocks down 95% of glutamate uptake into synaptosomes (Haugeto et al., 1996). Given its critical role in maintaining glutamate homeostasis, it is not surprising that abnormalities in GLT-1 expression and function have been implicated in numerous neurological disorders including: neuropsychiatric (addiction, schizophrenia) and neurodegenerative (amyotrophic lateral sclerosis, Huntington's disease, Parkinson's disease, Alzheimer's disease) disorders (Goursaud et al., 2008; Miller et al., 2008; Bellesi and Conti, 2010; Knackstedt et al., 2010; Massie et al., 2010; Zink et al., 2010; Mookherjee et al., 2011; Fischer et al., 2013).

Neuronal GLT-1

While previously thought to exist solely on astrocytes (Rothstein et al., 1994; Danbolt, 2001), the Rosenberg lab and others have identified GLT-1 as the major, if not only, glutamate transporter associated with excitatory terminals; specifically, the presence of GLT-1 mRNA and protein have been demonstrated in axon terminals within hippocampus, striatum, and somatosensory cortex (Berger and Hediger, 1998; Chen et al., 2004; Berger et al., 2005a; Furness et al., 2008; Petr et al., 2013). An understanding of the functional importance of

neuronal GLT-1 (nGLT-1) is lacking, as it has not been considered important for the regulation of glutamate homeostasis, primarily due to the fact that it accounts for only 5-10% of total GLT-1 expression (Furness et al., 2008). However, it is conceivable that this small percentage of GLT-1 expressed in excitatory terminals could critically contribute to the regulation of glutamate homeostasis, given the proximity to synaptic glutamate release and the high demand for glutamate uptake in preventing excitotoxicity via excessive glutamate receptor stimulation. A major goal of the Rosenberg lab has been to elucidate the functional significance of GLT-1 expressed in neurons in order to understand its role in maintaining glutamate homeostasis. In order to investigate these functions, the Rosenberg lab has generated a conditional GLT-1 KO mouse line where GLT-1 can be specifically deleted from neurons (Petr et al., 2015b).

Neuronal specific deletion of GLT-1

Multiple lines of research have been completed in order to determine what role, if any, nGLT-1 has on maintaining glutamate homeostasis and what biological consequences occur due to its deletion.

First, forebrain synaptosomal glutamate uptake was assessed in both nGLT-1 KO and astrocyte GLT-1 (aGLT-1) KO mice. Interestingly, nGLT-1, and not aGLT-1, was found to account for the majority of glutamate uptake (Petr et al., 2015b). This was the first finding to suggest that not only does nGLT-1 serve an important functional role in regulating *in vivo* glutamate homeostasis, but also that this role might be more critical than aGLT-1.

Second, multiple basic behavioral characterizations were completed; nGLT-1 KO mice were subjected to a variety of tests to assess locomotion, sensorimotor gating, sociability, cognitive function, and anxiety. As a whole, the nGLT-1 KO mouse demonstrated few abnormalities, which was interesting given the prior finding and that complete deletion of GLT-1 results in death via intractable seizures by six weeks of age (Tanaka et al., 1997). Overall, locomotion was unchanged in the nGLT-1 KO, however, automated gait analysis revealed a decrease in stride variability (unpublished findings). Differences in performance were revealed in the light-dark emergence, novel object recognition, and social interaction tasks (Fischer et al., 2015). Light-dark emergence is thought to be a test of anxiety based on the natural aversion of mice to light and on their exploratory and approach behavior. Novel object recognition is a visual learning task used to assess the ability of animals to recognize a novel object in a familiar environment. Social interaction is a test used to measure sociability. nGLT-1 KO mice spent significantly more time in the illuminated chamber in the light dark emergence task, more time exploring a novel object, and more time with a novel mouse in the social interaction task. Interestingly, they did not manifest evidence of increased anxiety, or deficits in cognitive functioning in other tests, such as open field, elevated plus maze, and fear conditioning, which may implicate nGLT-1 more in exploratory and approach behaviors.

Third, because locomotor responses to psychostimulants are modulated by glutamatergic signaling (Wolf, 1998), the nGLT-1 KO was tested for the locomotor effects of a d-amphetamine (AMP) challenge. Remarkably, we found a

significantly blunted response in the nGLT-1 KO to both acute and repeated administrations of AMP (Fischer et al., 2015).

Fourth, the effects of nGLT-1 and aGLT-1 KO on plasticity were assessed in the CA3-CA1 circuit. Complete knockout of GLT-1 results in the impairment in long-term potentiation (LTP) induction due to excessive activation of NMDA receptors (Katagiri et al., 2001), and thus the question is raised of whether GLT-1 expressed on neurons, astrocytes, or both is responsible. Interestingly, it was nGLT-1 KO, and not aGLT-1 KO, that recapitulated this impaired induction of plasticity (unpublished findings).

Aim

In contrast to the conventional thought, nGLT-1 has been established to play an important functional role in regulating glutamate homeostasis that could potentially be more critical than aGLT-1. Furthermore, deletion of nGLT-1 has been shown to result in disruptions in multiple biological phenomena. However, the full extent of the biological consequences of nGLT-1 KO is unknown. The aim of this project was to investigate the transcriptome profiles resultant from knockout of nGLT-1, within regions known to express GLT-1 on neurons, to identify and characterize alterations in known biological pathways.

Chapter 2

Materials and Methods

Subjects

nGLT-1 knockout mice were generated by insertion of loxP sites around exon 4 of the GLT-1 gene, as described earlier (Petr et al., 2015b). We crossed GLT-$1^{flox/flox}$ mice (on a mixed 129SvJ-C57BL/6 background) with a synapsin 1-cre (SynCre) transgenic mouse line (on a C57BL/6 background; JAX Stock No. 003966) that expresses Cre-recombinase under the neuron-specific promoter, synapsin 1. From this pairing, we obtained SynCre (+); GLT-1 floxed mice (neuron specific GLT-1 knockout mice), and SynCre (-); GLT-1 floxed mice (control mice). SynCre was introduced only through the females due to known cre expression in the testes (Rempe et al., 2006). All animal experiments were carried out in accordance with NIH guidelines, and were approved by the Children's Hospital Boston Institutional Animal Care and Use Committee. Animals were maintained on a 12-h light-dark cycle. Experiments were conduced on adult male mice 12 weeks of age, using age-matched littermates as controls. Food and water were available ad libitum.

Tissue preparation

Tissue was prepared from 4 nGLT-1 KO and 4 WT littermate control mice for RNA sequencing experiments. Briefly, mice were anesthetized (isoflurane

inhalation) and decapitated. Brains were rapidly removed, flash frozen in hexane chilled with dry ice, and stored at -80°C.

Following extraction of all brains, individual brains were positioned in a 1 mm coronal brain-sectioning matrix on ice and allowed to thaw only to the point that a razor blade could easily slice through without cracking (too cold) or compressing (to warm) the tissue. The brain was then rapidly sectioned with razor blades and each slice maintained on the individual slicing razor blade on dry ice. Regions of interest (including CA3, CA1, and dorsolateral Striatum) were dissected and stored at -80°C. All surfaces and implements, used here and for all subsequent steps involving nucleic acids, were thoroughly cleaned with 10% standard commercial bleach solution to prevent nucleic acid and RNase contamination (Prince and Andrus, 1992).

RNA isolation

Total RNA was isolated from tissue samples using a Qiagen miRNeasy Mini Kit (Cat. no. 217004). High quality RNA preparations are necessary for accurate quantification in RNA sequencing. Because total RNA preparations that exclude miRNAs artificially increase RNA quality control measurements [e.g. Agilent 2100 Bioanalyzer; RNA Integrity Number (RIN)], a preparation was utilized that included miRNAs in the total RNA recovery to ensure a more accurate RNA quality measurement.

Briefly, 700 µL of QIAzol reagent was added to each tissue sample, immediately homogenized with a rotor-stator homogenizer for 20-40 s, and incubated at RT

for 5 min. Then, 140 µL chloroform was added to the sample preparation, vortexed for 15 s, incubated at RT for 3 min, and centrifuged at 4°C at 12,000 x g for 15 min. Following centrifugation, the upper aqueous phase was extracted, combined with 1.5 volumes (~525 µL) of 100% ethanol, and thoroughly mixed. 700 µL sample volume was applied to a RNeasy Mini spin column and centrifuged at RT at 8,000 x g for 15 s to bind RNA to the column; this step was repeated for the remaining sample volume. The column was then washed with 500 µL Buffer RPE via centrifugation at RT at 8,000 x g for 15 s; this step was repeated with centrifugation for 2 min. Residual Buffer RPE was removed via centrifugation at RT at maximum speed for 1 min. Finally, 50 µL RNase-free water was applied directly onto the membrane of the column and centrifuged at RT at 8,000 x g for 1 min to elute RNA into a collection tube. 5 µL RNA solution was extracted for quality testing and the remainder was stored at -80°C until RNA sequencing library construction.

RNA quality and concentration were assessed via the Agilent 2100 Bioanalyzer system (MIT BioMicro Center). For each region and genotype, the top three RIN valued samples (minimum: RIN > 7.5) were utilized for subsequent RNA sequencing library construction and analyses.

RNA sequencing library construction

Single-end read sequencing libraries were constructed using an Illumina TruSeq RNA sample preparation kit v2 (Cat. no. RS-122-2002) according to the low

sample protocol. One region, including all nGLT-1 KO and WT biological replicates, was processed per run described as follows.

Purify and Fragment mRNA: First, for each sample, 0.5 µg total RNA (Illumina specification: 0.1 – 1.0 µg total RNA) was diluted with RNase-free water to a final volume of 50 µL and gently resuspended with 50 µL vigorously mixed RNA purification bead (oligo-dT) solution in a 0.3 mL well of a 96-well PCR plate. Once all samples were added, the PCR plate was sealed and placed into a thermocycler (C1000 Touch Thermal Cycler; BioRad). RNA/bead sample mixtures were cycled (65°C for 5 min, 4°C hold) to denature RNA and facilitate binding of polyA RNA to the purification beads and subsequently incubated at RT for 5 min to complete RNA-bead binding.

Next, the PCR plate was unsealed and incubated at RT for 5 min on a magnetic stand to separate polyA RNA bound beads from solution; the supernatant was then discarded and the PCR plate removed from the magnetic stand. The polyA RNA bound bead samples were resuspended in 200 µL Bead Washing Buffer and the PCR plate was again incubated at RT for 5 min on a magnetic stand; the supernatant (containing unbound ribosomal and other non-messenger RNA) was discarded and the PCR plate removed from the magnetic stand. The polyA RNA bound bead samples were resuspended in 50 µL Elution Buffer; the PCR plate was then sealed, placed into a thermocycler, and cycled (80°C for 2 min, 25°C hold) to elute the RNA (containing mRNA and any contaminant ribosomal RNA) from the beads.

Then, the PCR plate was unsealed and each sample resuspended in 50 µL Bead Binding Buffer, which favors specific mRNA-bead binding. Samples were incubated at RT for 5 min to complete mRNA-bead binding and subsequently incubated at RT for 5 min on a magnetic stand; the supernatant was then discarded and the PCR plate removed from the magnetic stand. PolyA mRNA bound bead samples were resuspended in 200 µL Bead Washing Buffer and the PCR plate was again incubated at RT for 5 min on a magnetic stand; the supernatant (containing residual ribosomal RNA and other contamination) was discarded and the PCR plate removed from the magnetic stand.

Finally, polyA mRNA bound bead samples were resuspended in 19.5 µL Elute, Prime, Fragment Mix; the PCR plate was then sealed, placed into a thermocycler, and cycled (94°C for 8 min, 4°C hold) to elute the mRNA from the beads, fragment the mRNA strands, as well as prime the mRNA fragments with random hexamers for subsequent first strand cDNA synthesis.

Synthesize First Strand cDNA: Following the prior thermocycling, the PCR plate was briefly centrifuged (5 s quick spin), unsealed, and incubated at RT for 5 min on a magnetic stand. 17 µL supernatant (fragmented and primed mRNA) from each sample was transferred to the corresponding 0.3 mL well of a new 96-well PCR plate. 60 µL SuperScript II – First Strand Master Mix (6 µL SuperScript II, 54 µL First Strand Master Mix; thoroughly resuspended) was prepared and 8 µL resuspended into each mRNA sample. The PCR plate was then sealed, placed into a thermocycler, and cycled (Pre-heat lid to 100°C, 25°C for 10 min, 42°C for 50 min, 70°C for 15 min, 4°C hold) to synthesize the first strand of cDNA.

Synthesize Second Strand cDNA: Following the prior thermocycling, the PCR plate was unsealed and 25 µL Second Strand Master Mix resuspended into each mRNA/cDNA sample; the PCR plate was then sealed and incubated in a pre-heated thermocycler (16°C, 1 h) to synthesize the complementary second strand of cDNA.

Next, the PCR plate was unsealed and incubated at RT for 2 min. 90 µL of thoroughly mixed AMPure XP beads were resuspended in each double stranded (ds) cDNA sample and incubated at RT for 15 min to complete cDNA-bead binding. The PCR plate was then incubated at RT for 5 min on a magnetic stand; 135 µL of supernatant was discarded. While on the magnetic stand, 200 µL 80% ethanol was added to each ds cDNA bound bead sample without disturbing the beads and allowed to incubate at RT for 30 s before supernatant was discarded; this process was repeated one additional time. Following the second supernatant extraction, the PCR plate was incubated at RT for 15 min to dry.

Finally, the PCR plate was removed from the magnetic stand, each ds cDNA bound bead sample resuspended in 52.5 µL Resuspension Buffer, and incubated at RT for 2 min to complete elution of ds cDNA from the AMPure XP beads. The PCR plate was incubated at RT for 5 min on a magnetic stand; subsequently 50 µL of supernatant (ds cDNA) was transferred to the corresponding 0.3 mL well on a new 96-well PCR plate.

Perform End Repair: 10 µL Resuspension Buffer and 40 µL End Repair Mix were resuspended into each ds cDNA sample. The PCR plate was sealed and

incubated on a pre-heated thermocycler (30°C, 30 min) to convert overhangs from fragmentation into blunt ends.

Following incubation, the PCR plate was unsealed and 160 µL of thoroughly mixed AMPure XP beads were resuspended in each ds cDNA sample and incubated at RT for 15 min to complete ds cDNA-bead binding. The PCR plate was then incubated at RT for 5 min on a magnetic stand; 127.5 µL supernatant was discarded. While on the magnetic stand, 200 µL 80% ethanol was added to each ds cDNA bound bead sample without disturbing the beads and allowed to incubate at RT for 30 s before supernatant was discarded; this process was repeated one additional time. Following the second supernatant extraction, the PCR plate was incubated at RT for 15 min to dry.

Finally, the PCR plate was removed from the magnetic stand, each ds cDNA bound bead sample resuspended in 17.5 µL Resuspension Buffer, and incubated at RT for 2 min to complete elution of ds cDNA from the AMPure XP beads. The PCR plate was incubated at RT for 5 min on a magnetic stand; subsequently 15 µL of supernatant (ds cDNA) was transferred to the corresponding 0.3 mL well on a new 96-well PCR plate.

Adenylate 3' Ends: 2.5 µL Resuspension Buffer and 12.5 µL A-Tailing Mix was resuspended into each ds cDNA sample. The PCR plate was sealed, placed in a thermocycler, and cycled (Pre-heat lid to 100°C, 37°C for 30 min, 70°C for 5 min, 4°C hold) to adenylate 3' ends, which introduces a single nucleotide (NT) overhang for the subsequent adapter ligation and prevents cross ds cDNA ligation.

Ligate Adapters: Prior to adapter ligation, unique 6 NT adapters were assigned to each sample to maintain sample hybridization segregation during down-stream RNA sequencing. Following the prior thermocycling, the PCR plate was unsealed and 2.5 µL resuspension buffer as well as 2.5 µL Ligation Mix were resuspended in each ds cDNA sample. In addition, 2.5 µL of the assigned unique RNA Adapter Index was resuspended in each sample. The PCR plate was sealed and incubated in a pre-heated thermocycler (30°C, 10 min) to complete adapter ligation.

Next, the PCR plate was unsealed and 5 µL Stop Ligation Buffer resuspended in each sample to inactivate the ligation. 42 µL thoroughly mixed AMPure XP beads were resuspended into each sample and incubated at RT for 15 min to complete ds cDNA-bead binding. The PCR plate was then incubated at RT for 5 min on a magnetic stand; 79.5 µL of supernatant was discarded. While on the magnetic stand, 200 µL 80% ethanol was added to each ds cDNA bound bead sample without disturbing the beads and allowed to incubate at RT for 30 s before supernatant was discarded; this process was repeated one additional time. Following the second supernatant extraction, the PCR plate was incubated at RT for 15 min to dry. The PCR plate was removed from the magnetic stand, each ds cDNA bound bead sample resuspended in 52.5 µL Resuspension Buffer, and incubated at RT for 2 min to complete elution of ds cDNA from the AMPure XP beads. The PCR plate was incubated at RT for 2 min on a magnetic stand; subsequently 50 µL of supernatant (ds cDNA) was transferred to the corresponding 0.3 mL well on a new 96-well PCR plate.

A second cleanup was then completed to thoroughly remove any residual contamination. 50 µL thoroughly mixed AMPure XP beads were resuspended into each sample and incubated at RT for 15 min to complete ds cDNA-bead binding. The PCR plate was then incubated at RT for 5 min on a magnetic stand; 95 µL of supernatant was discarded. While on the magnetic stand, 200 µL 80% ethanol was added to each ds cDNA bound bead sample without disturbing the beads and allowed to incubate at RT for 30 s before supernatant was discarded; this process was repeated one additional time. Following the second supernatant extraction, the PCR plate was incubated at RT for 15 min to dry. The PCR plate was removed from the magnetic stand, each ds cDNA bound bead sample resuspended in 22.5 µL Resuspension Buffer, and incubated at RT for 2 min to complete elution of ds cDNA from the AMPure XP beads. The PCR plate was incubated at RT for 2 min on a magnetic stand; subsequently 20 µL of supernatant (adapter ligated ds cDNA) was transferred to the corresponding 0.3 mL well on a new 96-well PCR plate.

Enrich DNA Fragments: 5 µL PCR Primer Cocktail (specific to the adapters) and 25 µL PCR Master Mix were resuspended in each ds cDNA sample. The PCR plate was sealed, placed into a thermocycler, and cycled [Pre-heat lid to 100°C, 98°C for 30 s, (98°C for 10 s, 60°C for 30 s, 72°C for 30 s) x 15, 72°C for 5 min, 10°C hold] to selectively amplify ds cDNA containing adapters on both ends. Next, the PCR plate was unsealed and 50 µL thoroughly mixed AMPure XP beads were resuspended into each sample and incubated at RT for 15 min to complete ds cDNA-bead binding. The PCR plate was then incubated at RT for 5

min on a magnetic stand; 95 µL of supernatant was discarded. While on the magnetic stand, 200 µL 80% ethanol was added to each ds cDNA bound bead sample without disturbing the beads and allowed to incubate at RT for 30 s before supernatant was discarded; this process was repeated one additional time. Following the second supernatant extraction, the PCR plate was incubated at RT for 15 min to dry. The PCR plate was removed from the magnetic stand, each ds cDNA bound bead sample resuspended in 32.5 µL Resuspension Buffer, and incubated at RT for 2 min to complete elution of ds cDNA library from the AMPure XP beads. The PCR plate was incubated at RT for 5 min on a magnetic stand; subsequently 30 µL of supernatant (ds cDNA library) was transferred to the corresponding 0.3 mL well on a new 96-well PCR plate. Sample libraries were stored at -80°C until RNA sequencing.

Validate Library: Library quality was confirmed using an Advanced Analytical Fragment Analyzer and quantified by qPCR before pooling (MIT BioMicro Center). All samples passed library validation and were used for subsequent RNA sequencing.

RNA sequencing

RNA sequencing was performed at the MIT BioMicro Center using an Illumina HiSeq 2000 with 40 NT single-end reads. Three flow cell lanes were multiplexed according to sample region (Regions: CA3, CA1, and Striatum; Biological Replications: 3 nGLT-1 KO and 3 WT). Data were acquired and processed through the BioMicro Center BMC/BCC 1.0.2 pipeline. Data were demultiplexed

using custom scripts allowing for one mismatch and quality was checked using Illumina SAV and FastQC. Generated FASTQ files containing unmapped sequencing reads (15 million – 32 million reads per sample) were utilized for the downstream analysis pipeline.

RNA sequencing analysis pipeline

Sequencing data were processed using the Tophat – Cufflinks read mapping, transcriptome assembly, and differential expression analysis pipeline (Trapnell et al., 2009, 2010, 2013; Roberts et al., 2011a, 2011b; Kim et al., 2013). All analyses were conducted through a web-based Galaxy bioinformatics computing platform (http://usegalaxy.org; v.2.2.1.2) (Goecks et al., 2010).

Tophat: Sequencing read alignment was conducted using Tophat (v.2.0.14). Tophat is a fast splice junction-mapping tool that aligns sequencing reads to a reference genome using the short read aligner Bowtie (v.2.2.5) and subsequently identifies exon-exon splice junctions from the resulting read mapping (Trapnell et al., 2009; Kim et al., 2013). Here, sequencing reads were mapped to the UCSC mm10 reference genome without novel transcript detection. Tophat parameters were adjusted based on the experimental RNA sequencing methodology. Adjusted settings are as follows (note: settings not indicated were run at default values):

- Maximum realign edit distance = 0
- Number of mismatches allowed in each segment for reads mapped independently = 1

- Minimum length of read segments = 20
- Output unmapped reads = True
- Supply your own junction data = True
    - Use gene annotation model = True
        - iGenomes UCSC mm10 reference annotation
    - Only look for supplied junctions = True
- Set Bowtie 2 settings = True
    - Very sensitive

Cufflinks: Transcriptome assembly was conducted using Cufflinks (v.2.2.1). Cufflinks assembles individual transcripts from genome-mapped sequencing reads using a reference transcriptome annotation, accounting for alternative splicing structure. Because many genes have multiple splice variants, multiple transcript reconstructions are possible that account for the set of mapped reads. Therefore, the cufflinks algorithm identifies the set with the fewest full-length transcript fragments necessary to explain the input mapped reads. Following transcriptome assembly, cufflinks estimates the abundance of all full-length transcript fragments while identifying and removing artifacts (Trapnell et al., 2010, 2013; Roberts et al., 2011b). Here, transcriptome assembly was conducted using the iGenomes UCSC reference transcriptome annotation. Cufflinks parameters were adjusted based on the experimental RNA sequencing methodology as well as the Tophat read mapping procedure. Adjusted settings are as follows (note: settings not indicated were run at default values):

- Perform bias correction = True
    - UCSC mm10 reference genome
- Use multi-read correct = True
- Max maximum likelihood estimation iterations = 50,000

Cuffmerge: Merging of transcriptome assemblies for each sample region was conducted using Cuffmerge (v.2.2.1). In order to conduct differential gene expression analysis, it is necessary to obtain a pooled set of all transcripts (Trapnell et al., 2010, 2013; Roberts et al., 2011b). However, pooling all mapped reads for transcriptome assembly increases computational demand and increases the probability of incorrect transcript assembly due to more complex mixture of alternative splicing structures. Cuffmerge functions as a second-level transcriptome assembler, merging the input assembled transcript fragments in the most parsimonious manner, similar to cufflinks treatment of input mapped reads. Additionally, a reference annotation-based transcript assembly is performed with a reference transcriptome annotation to merge reference transcripts and sample transcript fragments to output a single annotation file for use in the subsequent differential expression analysis. Here, transcriptome merging was conducted using the iGenomes UCSC mm10 reference transcriptome annotation as well as the UCSC mm10 reference genome to incorporate additional gene classifying information. All additional parameters were run as default.

Cuffdiff: Differential expression analysis was conducted using Cuffdiff (v.2.2.1). Cuffdiff calculates expression values in and determines statistical significance of observed expression changes between two or more sample groups (Trapnell et al., 2010, 2013; Roberts et al., 2011b). It is assumed that the number of transcript reads are proportional to its abundance, but that these reads fluctuate between replicates due to technical and biological variability. Cuffdiff utilizes technical and/or biological replicates to estimate this variability in read counts for each gene and uses this information to determine statistical significance of observed expression changes. In addition, inherent bias, such as those commonly resulting from library preparation protocols (Levin et al., 2010; Li et al., 2010), are modeled and corrected to improve abundance calculations. Cuffdiff outputs multiple data files that are utilized in downstream data exploration and visualization in CummeRbund. Here, differential expression analysis was conducted for each region using Tophat mapped reads and associated Cuffmerge merged transcriptome. Cuffdiff parameters were adjusted based on the experimental RNA sequencing methodology as well as the Tophat read mapping and Cufflinks transcriptome assembly procedures. Adjusted settings are as follows (note: settings not indicated were run at default values):

- Use multi-read correct = True
- Perform bias correction = True
    - UCSC mm10 reference genome
- Include read group datasets = True
- Include count based output files = True

- Max maximum likelihood estimation iterations = 50,000

CummeRbund: Data exploration and visualization was conducted in CummeRbund (v.2.10.0) in the R (v.3.2.1) environment (Trapnell et al., 2012). Database files were generated for each Cuffdiff analysis (CA3, CA1, and Striatum) and figures outlining key results related to the differential expression analysis were created.

Pathway analysis

Differential expression analyses of RNA sequencing data offer an important starting point for determining biological consequences of experimental perturbations (e.g. KO of nGLT-1 as presented here). It is next critical to provide biological context to the differential gene expression profile using the known literature regarding biological processes and states to start dissecting these important biological consequences; Gene Set Analysis (GSA) is a commonly utilized and robust strategy (Luo et al., 2009). Here, GSA was conducted using the Generally Applicable Gene-Set (GAGE) pathway analysis (Luo et al., 2009) utilizing the Kyoto Encyclopedia of Genes and Genomes (KEGG) mouse pathway database (Ogata et al., 1999).

GAGE pathway analysis (v.2.18.0) was conducted in the R (v.3.2.1) environment according to the *RNA-Seq Data Pathway and Gene-set Analysis Workflow* Bioconducter vignette (April 16th, 2015), with modification. GAGE analyses were run by region; Tophat mapped reads for the corresponding samples were run

using the aforementioned computational workflow with the exceptions that it was set to single-end reads and without paired-end read bam file parameters. Two analyses were run per region: single direction, whereby pathways were assessed based on identical direction in gene expression changes (i.e. either all up-regulated or all down-regulated), and dual direction, whereby pathways were assessed based on significant gene expression changes in either direction. Analysis output was visualized with Pathview (v.1.8.0) in the R (v.3.2.1) environment (Luo and Brouwer, 2013) according to the aforementioned computational workflow. Figures of significant KEGG pathways were generated, overlaying gene expression data onto corresponding KEGG diagrams.

Statistics

All statistical p-values were corrected for multiple testing using the Benjamini-Hochberg procedure (); resultant q-values were used for determining statistical significance. Statistical significance was defined as $q < 0.05$ for Cuffdiff differential expression analyses and as $q < 0.10$ for GAGE pathway analyses.

Chapter 3

Results

CA3

GLT-1 protein expressed in neurons is primarily localized to the pre-synaptic terminal (Chen et al., 2002, 2004). If nGLT-1 plays an important functional role in maintaining synaptic glutamate homeostasis, then its functional deletion would likely have direct biological consequences at both the pre- and post-synaptic neurons as well as at synaptic-associated glial cells. Projection neurons in area CA3 of the hippocampus are known to highly express GLT-1 (Chen et al., 2004); in addition to projecting to area CA1 of the hippocampus, these neurons also form recurrent synaptic connections within CA3 (Ishizuka et al., 1990; Li et al., 1994). Given that CA3 abundantly contains neurons expressing GLT-1 as well as post-synaptic neurons and glial cells that would be modulated by a functional role for nGLT-1 in controlling glutamate homeostasis, any biological effects resulting from deletion of nGLT-1 would be most likely to occur here.

Differential gene expression analysis was conducted through the Tophat – Cufflinks pipeline (Trapnell et al., 2009, 2010, 2013; Roberts et al., 2011a, 2011b; Kim et al., 2013). Initially, three biological replicates were included for each condition (3 nGLT-1 KO and 3 WT). However, analyses indicated that one of the nGLT-1 KO replicates (nKO-Fail) failed to pass quality control. First, nKO-Fail displayed a greater squared coefficient of variance (CV^2) for all FPKM (fragments per kilobase of transcript per million mapped reads; normalized

fragment count for each gene based on the full length transcript) values (data not shown) compared to the other nGLT-1 KO and WT replicates; the increased variability disrupts the quantification estimation and significance calculation processes during the Cufflinks-Cuffmerge-Cuffdiff analysis (Trapnell et al., 2010, 2013; Roberts et al., 2011b). Second, nKO-Fail clustered with WT replicates according to a principal component analysis and confirmed with a Jensen-Shannon distance analysis (data not shown). Similar quality control findings for nKO-Fail were found in the CA1 and Striatum analyses and, thus, nKO-Fail was removed from all analyses. It is unknown whether biological or technical issues invalidated this sample; however, one possibility is that there was inefficient or incomplete cre-mediated inactivation of GLT-1 in neurons (Schulz et al., 2007). Global analysis within CA3 samples of the 2 nGLT-1 KO and 3 WT replicates indicated that all replicates passed quality control for the Cufflinks-Cuffmerge-Cuffdiff analysis. Variance analysis indicates no differences in the CV^2 vs. FPKM values between nGLT-1 KO and WT replicates (**Figure 1**). In addition, nGLT-1 KO and WT replicates displayed a well-defined segregation of clustering according to principal component analysis (**Figure 2**).

Gene expression analysis revealed 1509 differentially expressed genes within CA3 between nGLT-1 KO and WT groups ($q < 0.05$). Differentially expressed genes are visualized with non-significantly altered genes in **Figure 3** [$-\log_{10}$(p-value) vs. $\log_2$(fold change in expression)]. Replicate FPKM values for all differentially expressed genes are visualized in **Figure 4**.

GAGE (Luo et al., 2009) and Pathview (Luo and Brouwer, 2013) were utilized to analyze gene expression results to identify significantly enriched KEGG mouse biological pathways. Single-direction GAGE analysis revealed a significant up-regulation in the oxidative phosphorylation pathway ($t = 4.673$; $q = 2.80*10^{-8}$; set size = 117) (**Figure 5**). Dual-direction GAGE analysis revealed a significant change in the KEGG calcium signaling ($t = 2.784$; $q = 3.18*10^{-3}$; set size = 178) (**Figure 6**) and neuroactive ligand-receptor interaction ($t = 4.051$; $q = 1.46*10^{-6}$; set size = 260) (**Figure 7**) pathways.

CA1

Area CA1 of the hippocampus contains high expression of GLT-1 protein in axon terminals of glutamatergic pyramidal neurons originating in CA3 (Chen et al., 2004). Thus, CA1 is an ideal region to investigate the biological consequences of nGLT-1 deletion specifically in post-synaptic neurons and glial cells that could be directly modulated by a functional role for nGLT-1 in regulating synaptic glutamate homeostasis.

Global analysis within CA1 samples of the 2 nGLT-1 KO and 3 WT replicates indicated that all replicates passed quality control for the Cufflinks-Cuffmerge-Cuffdiff analysis. Variance analysis indicate only slight differences in the CV^2 vs. FPKM values between nGLT-1 KO and WT replicates, isolated primarily to lower FPKM values (**Figure 8**). However, nGLT-1 KO and WT replicates did not display well-defined segregation of clustering according to principal component analysis (**Figure 9**). KO_0 was more closely related to the WT_1 and WT_2 replicates

than to the KO_1 replicate. While these results likely negatively impacted the Cufflinks-Cuffmerge-Cuffdiff analysis (i.e. more stringent significance threshold leading to fewer differentially expressed genes) (Trapnell et al., 2010, 2013; Roberts et al., 2011b), there was not enough compelling data to remove KO_0 from the analysis, as the clustering could be indicative of the true biological environment.

Gene expression analysis revealed 322 differentially expressed genes within CA1 between nGLT-1 KO and WT groups ($q < 0.05$). Differentially expressed genes are visualized with non-significantly altered genes in **Figure 10** [$-\log_{10}$(p-value) vs. $\log_2$(fold change in expression)]. Replicate FPKM values for all differentially expressed genes are visualized in **Figure 11**.

GAGE and Pathview were utilized to analyze gene expression results to identify significantly enriched KEGG mouse biological pathways. Dual-direction GAGE analysis revealed significant changes in the KEGG calcium signaling ($t = 2.598$; $q = 6.84*10^{-3}$; set size = 178) (**Figure 12**) and neuroactive ligand-receptor interaction ($t = 4.436$; $q = 6.15*10^{-8}$; set size = 255) (**Figure 13**) pathways.

Striatum

The striatum receives dense glutamatergic pyramidal neuron input, primarily originating from cortical layer V (Wilson, 1987; Bennett and Bolam, 1994). Interestingly, GLT-1 is expressed in cortical neurons, with the highest levels of expression occurring in layer V and VI (Berger and Hediger, 1998; Berger et al., 2005b). Recently, the Rosenberg lab found extensive GLT-1 expression in axon

terminals within striatum (Petr et al., 2013). As with CA1, striatum is an ideal region to begin isolating the potential biological effects of nGLT-1 KO on post-synaptic neurons and glial cells; however, unlike CA1, the striatum contains primarily GABAergic projection neurons (~95% medium spiny neurons) (Chesselet et al., 2007; Berke, 2011), which could potentially be differentially regulated by nGLT-1 compared to glutamatergic projection neurons found in CA1.

Global analysis within Striatum samples of the 2 nGLT-1 KO and 3 WT replicates indicated that all replicates passed quality control for the Cufflinks-Cuffmerge-Cuffdiff analysis. Variance analysis indicates no differences in the CV^2 vs. FPKM values between nGLT-1 KO and WT replicates (**Figure 14**). In addition, nGLT-1 KO and WT replicates displayed segregation of clustering according to principal component analysis (**Figure 15**); note that KO_0 and KO_1 had a significant distance in clustering, however, because WT and KO groups were segregated and CV^2 vs. FPKM results were consistent, there was no compelling data to alter the replicates, as the clustering was likely indicative of the true biological environment.

Gene expression analysis revealed 1268 differentially expressed genes within CA3 between nGLT-1 KO and WT groups ($q < 0.05$). Differentially expressed genes are visualized with non-significantly altered genes in **Figure 16** [$-\log_{10}$(p-value) vs. $\log_2$(fold change in expression)]. Replicate FPKM values for all differentially expressed genes are visualized in **Figure 17**.

GAGE and Pathview were utilized to analyze gene expression results to identify significantly enriched KEGG mouse biological pathways. Single-direction GAGE analysis revealed a significant up-regulation in the oxidative phosphorylation pathway ($t = 1.999$; $q = 9.65*10^{-2}$; set size = 117) (**Figure 18**). Dual-direction GAGE analysis revealed a significant change in the KEGG calcium signaling ($t = 4.309$; $q = 1.14*10^{-7}$; set size = 178) (**Figure 19**) and neuroactive ligand-receptor interaction ($t = 5.789$; $q = 1.22*10^{-13}$; set size = 251) (**Figure 20**) pathways. In addition, specific neurotransmitter system pathways were perturbed. glutamatergic synapse ($t = 3.302$; $q = 9.66*10^{-5}$; set size = 111) (**Figure 21**); GABAergic synapse ($t = 2.200$; $q = 9.27*10^{-3}$; set size = 87) (**Figure 22**); dopaminergic synapse ($t = 1.888$; $q = 2.89*10^{-2}$; set size = 127) (**Figure 23**); retrograde endocannabinoid signaling ($t = 3.263$; $q = 1.10*10^{-4}$; set size = 101) (**Figure 24**); cholinergic synapse ($t = 2.710$; $q = 1.82*10^{-3}$; set size = 112) (**Figure 25**); and serotonergic synapse ($t = 2.649$; $q = 1.99*10^{-3}$; set size = 119) (**Figure 26**).

Chapter 4

Discussion

Overview of main findings

Here, I report that deletion of nGLT-1 results in a high degree of differential gene expression within CA3 (1509), CA1 (322), and Striatum (1268). Furthermore, these alterations in gene expression were enriched in KEGG annotated biological pathways related to energy metabolism and neurotransmission. These findings are surprising given that GLT-1 protein in neurons represents only about 5-10% of the overall total GLT-1 protein in the brain (Furness et al., 2008) and further supports the idea that nGLT-1 serves a critical role in the regulation of synaptic glutamate homeostasis.

Oxidative phosphorylation

Knockout of nGLT-1 results in a significant up-regulation of the KEGG oxidative phosphorylation pathway within CA3 and Striatum. Oxidative phosphorylation is a process by which high energy electrons, originating from carbon oxidations, are transferred via NADH through the mitochondrial electron transport chain complex to produce ATP, the primary cellular energy source (Knowles, 1980; Smeitink et al., 2001).

GLT-1 mediated glutamate uptake is powered by ion gradients; specifically, 1 glutamate molecule is transported via GLT-1 from the extracellular space to the cytosol through the counter-transport of 3 K^+ and 1 H^+ as well as the co-transport

of 1 K^+ (Levy et al., 1998). Because it accounts for ~1% of total brain protein (Lehre and Danbolt, 1998) and is essential in maintaining appropriate excitatory transmission and brain function (Tanaka et al., 1997), GLT-1 utilizes a substantial amount of ion gradient energy (Genda et al., 2011). Therefore, in order to power GLT-1 function, the cell must actively maintain the ion gradient; this is accomplished via the Na^+/K^+-ATPase (Rose et al., 2009). Interestingly, GLT-1 directly associates with Na^+/K^+-ATPase in a macromolecular complex and Na^+/K^+-ATPase function is required for GLT-1 mediated glutamate uptake (Rose et al., 2009).

In order for the Na^+/K^+-ATPase, and by extension GLT-1, to function, ATP must be readily available to meet the energy demands of glutamate uptake. In addition to Na^+/K^+-ATPase, GLT-1 also co-compartmentalizes with glycolytic enzymes and mitochondria (Genda et al., 2011); simultaneous disruption, but not either alone, of glycolysis and oxidative phosphorylation impairs GLT-1 function, indicating redundant energy source mechanisms for GLT-1 (Genda et al., 2011). Moreover, mitochondria migrate to GLT-1 in regions of increased neuronal activity in response to increased energy demand for glutamate clearance (Jackson et al., 2014).

Because oxidative phosphorylation genes are up-regulated in the nGLT-1 KO, it is likely the case that cells (neurons, astrocytes, or both) are compensating for the increased energy demand due to increased extracellular glutamate availability; future studies should assess the association of oxidative phosphorylation and mitochondria with nGLT-1, specifically.

In the context of neurological disease states, oxidative phosphorylation gene dysfunction has been implicated in neurodegenerative diseases such as Parkinson's Disease (PD) (Finsterer et al., 2001) and Alzheimer's Disease (AD) (Shoffner, 1997). Given a change in the oxidative phosphorylation pathway, one might expect to see behavioral alterations relevant to these disorders. In fact, the Rosenberg lab has uncovered behavioral differences in the nGLT-1 KO that suggest a resilient state to both PD and AD. First, a hallmark of PD is an abnormal gait that is, in part, characterized by increased variability (Yogev et al., 2007; Wang et al., 2012). We have found a significant decrease in variability in automated measures of gait (opposite direction of the PD phenotype) in the nGLT-1 KO compared to WT (unpublished findings). Second, AD is characterized by cognitive impairments related to learning and memory (Small et al., 2011). We have found a significant increase in novel object recognition (opposite direction of the AD phenotype) in the nGLT-1 KO compared to WT (unpublished findings). While these findings do not necessarily suggest a full resilience to either PD or AD, they are at least consistent with, and give potential context to, the oxidative phosphorylation result here.

Calcium signaling and neuroactive ligand-receptor interaction

Knockout of nGLT-1 results in a significant dual-direction enrichment of the KEGG calcium signaling and neuroactive ligand-receptor interaction pathways within CA3, CA1, and Striatum. Ca^{2+} is a critical component of many diverse signal transduction networks found in biology (Clapham, 2007).

In the nervous system, Ca^{2+} has many important functions directly related to neurotransmission (Berridge, 1998). For example, once an action potential reaches the axon terminal, voltage-gated Ca^{2+} influx triggers the exocytosis of synaptic vesicles, resulting in the release of neurotransmitter (Cousin and Robinson, 1999). Once released into the synaptic cleft, the neurotransmitters bind their cognate receptors, many of which are ionotropic and allow the passage of Ca^{2+} from the extracellular space into the cytosol (Dong et al., 2009). Here, the Ca^{2+} can initiate signaling cascades that allow the cell to respond to external stimuli (Berridge, 1998).

Neuronal plasticity, a subset of these signaling mechanisms, is particularly relevant to disruption in glutamate homeostasis and calcium signaling. LTP is a form of neuronal plasticity, usually mediated by Ca^{2+} influx, in response to high-frequency trains of stimulation (Lynch, 2004). The prototypical model of Ca^{2+}-induced LTP is conducted in the CA3-CA1 circuit. High-frequency tetanic stimulation of the CA3-CA1 Schaffer Collaterals results in a rapid buildup of glutamate in and around synaptic clefts in CA1. This glutamate buildup is sufficient to depolarize the post-synaptic neuron as well as unblock and activate NMDA receptors, allowing for the rapid influx of Ca^{2+}. This Ca^{2+} influx initiates a signaling cascade that increases AMPA receptor expression in the post-synaptic membrane and potentiates the response to further stimulation (Lynch, 2004). Enrichment of the calcium signaling and neuroactive-ligand receptor pathways presented here gives support to the idea that nGLT-1 serves an important functional role in maintaining synaptic glutamate homeostasis. Two additional

lines of evidence generated by the Rosenberg lab are consistent with these findings. First, nGLT-1 was found to be responsible for the majority of synaptosomal glutamate uptake (Petr et al., 2015a); while this finding is not necessarily indicative of the *in vivo* physiological environment, it is consistent with the *in vivo* snapshot of pathway enrichment. Second, complete GLT-1 KO results in deficient LTP induction due to excessive activation of NMDA receptors (Katagiri et al., 2001). Utilizing both the nGLT-1 KO and astrocyte-specific GLT-1 KO, the Rosenberg lab found that CA3-CA1 LTP induction is impaired in the nGLT-1 KO, but not the astrocyte GLT-1 KO (unpublished findings). The findings presented here suggest this to be due to aberrant calcium signaling due to disrupted neurotransmission, likely at the NMDA receptor; future studies will assess the hypothesis that the impairment in CA3-CA1 LTP induction in the nGLT-1 KO is due to excessive activation of NMDA receptors, recapitulating the full GLT-1 KO phenotype, resulting in disrupted calcium signaling.

Disruption in specific neurotransmitter systems within striatum

Knockout of nGLT-1 results in a significant dual-direction enrichment of the KEGG glutamatergic, GABAergic, dopaminergic, cholinergic, and serotonergic synapse as well as retrograde endocannabinoid signaling pathways within Striatum. These findings, representing disruptions in multiple neurotransmitter systems due to nGLT-1 KO, strongly support the idea that nGLT-1 is playing a critical role in regulating synaptic glutamate homeostasis.

In the context of the behavioral phenotype of the nGLT-1 KO, these findings are consistent with the recent and remarkable finding that nGLT-1 KO results in a blunted locomotor response to AMP (Fischer et al., 2015). Repeated administration of AMP leads to an augmentation of its behavioral effects, a process termed sensitization, and is associated with increased dopamine transmission within projection areas of the ventral tegmental area (VTA), particularly the ventral striatum (Robbins and Everitt, 1996; Bowers et al., 2010). Additionally, acute and chronic AMP administration increases glutamate transmission in striatum (Wolf, 1998), which is required for the sensitization effect (Burns et al., 1994; Wolf, 1998; David and Abraini, 2003). Furthermore, the GABA (Cedillo and Miranda, 2013), acetylcholine (Bickerdike and Abercrombie, 1997), serotonin (Przegaliński et al., 2000) and cannabinoid (Thiemann et al., 2008) neurotransmitter systems in striatum have all been implicated in regulating the behavioral response to AMP. While these findings are unable to determine any specific functional role for nGLT-1 in modulating these neurotransmitter systems within striatum, the results add a new layer of understanding to the AMP behavioral phenotype present in the nGLT-1 KO that has opened new avenues of research to pursue in future studies relating glutamate transport to other neurotransmitter systems.

Conclusions

Here, I demonstrate that knockout of nGLT-1 results in extensive differential gene expression and, consequently, enrichment of important neurobiological

signaling pathways directly related to energy metabolism and neurotransmission within regions currently known to express GLT-1 on axon terminals. These findings challenge the long-held assumption that, because GLT-1 expression on neurons is significantly lower than on astrocytes, nGLT-1 contributes little to the regulation of synaptic glutamate homeostasis. While the mechanisms underlying these results are currently unknown, future work will be guided by these findings to determine the specific biological functions of nGLT-1.

Figures

CA3

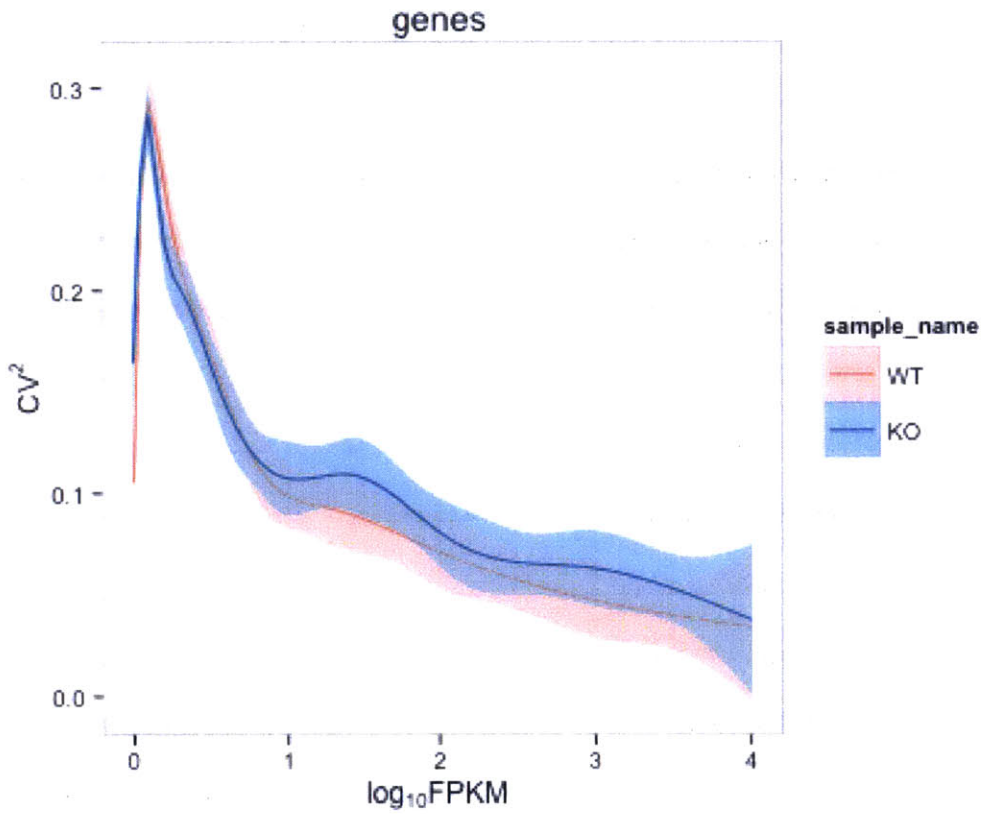

Figure 1: Variance analyses comparing CV^2 vs. $log_{10}FPKM$ values for all identified genes in nGLT-1 KO (KO; N = 2) and WT littermate control (WT; N = 3) CA3 samples. No differences in CV^2 vs. $log_{10}FPKM$ values were found. CV^2 = squared coefficient of variance; FPKM = fragments per kilobase of transcript per million mapped reads.

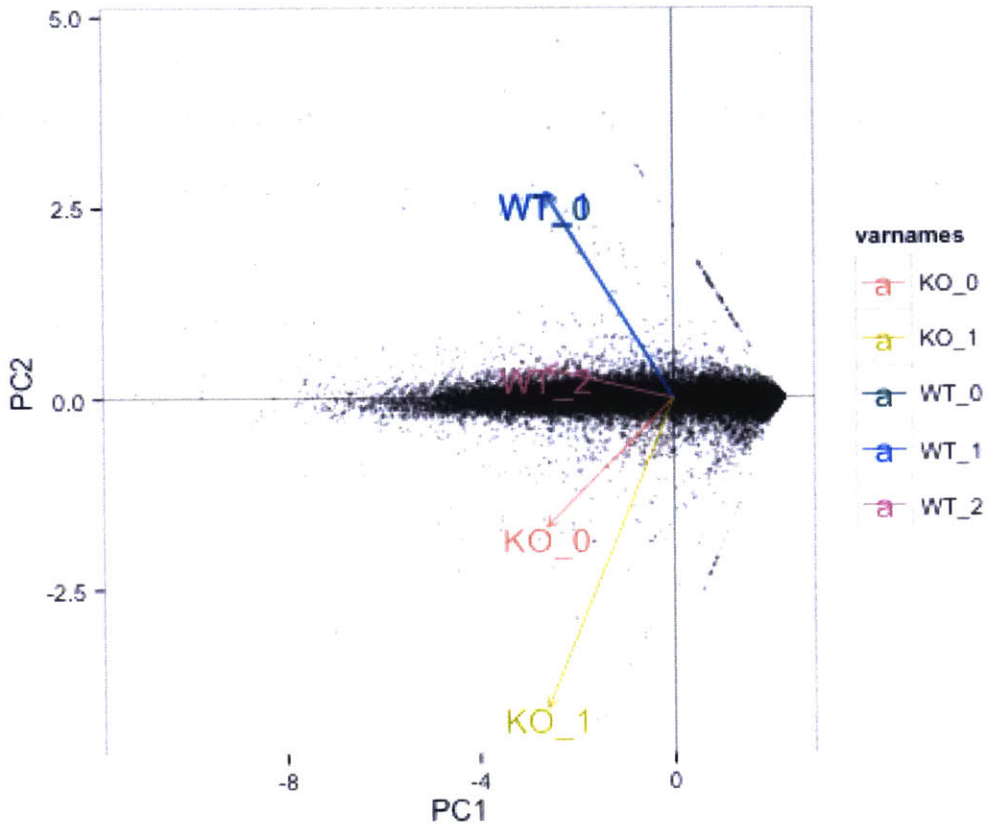

Figure 2: Principal Component Analysis comparing clustering of replicates over all identified genes in nGLT-1 KO (KO_0, KO_1) and WT littermate control (WT_0, WT_1, WT_2) CA3 samples. Distinct segregation of clustering was observed between nGLT-1 KO and WT replicates. PC1 = Principal Component 1; PC2 = Principal Component 2.

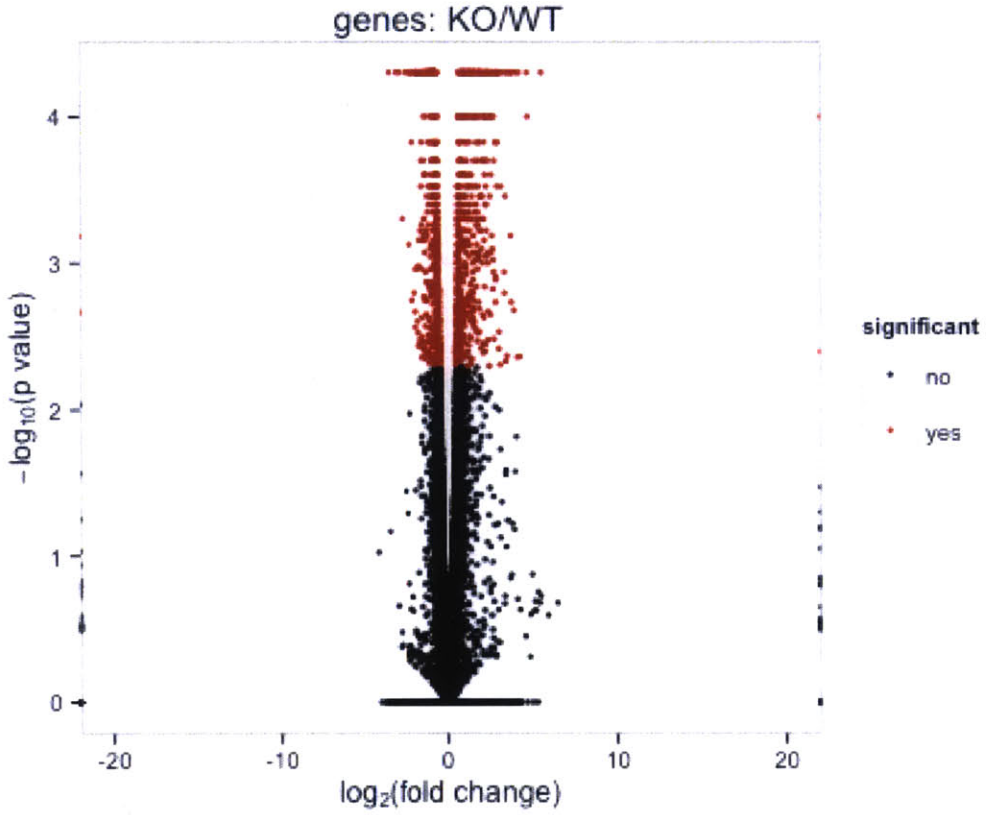

Figure 3: Volcano plot visualization of $-\log_{10}$(p-value) vs. $\log_2$(fold change in expression) for all identified genes in nGLT-1 KO (KO; N = 2) and WT littermate control (WT; N = 3) CA3 samples. Cuffdiff analysis revealed 1509 differentially expressed genes ($q < 0.05$). Significant genes are indicated in red and non-significant genes are indicated in black. P-values correspond to the original, uncorrected statistical value; fold change corresponds to the KO/WT ratio of mean expression values for a given gene.

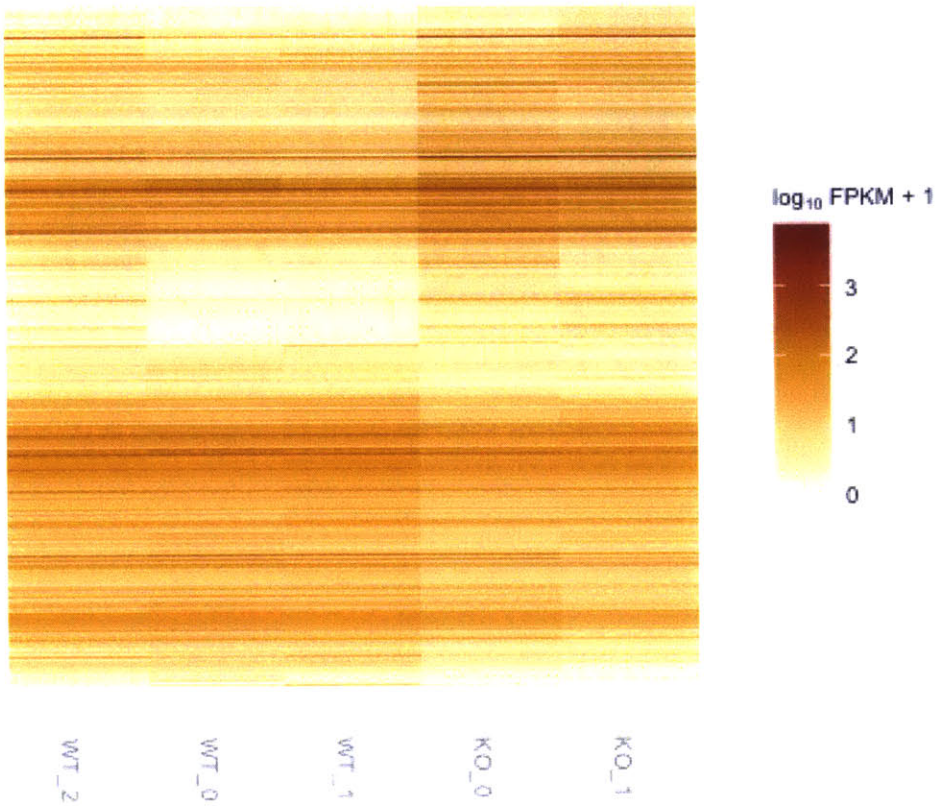

Figure 4: Heat map visualization of FPKM values for all replicates for all differentially regulated genes in nGLT-1 KO (KO_0, KO_1) and WT littermate control (WT_0, WT_1, WT_2) CA3 samples. Cuffdiff analysis revealed 1509 differentially expressed genes ($q < 0.05$). FPKM = fragments per kilobase of transcript per million mapped reads.

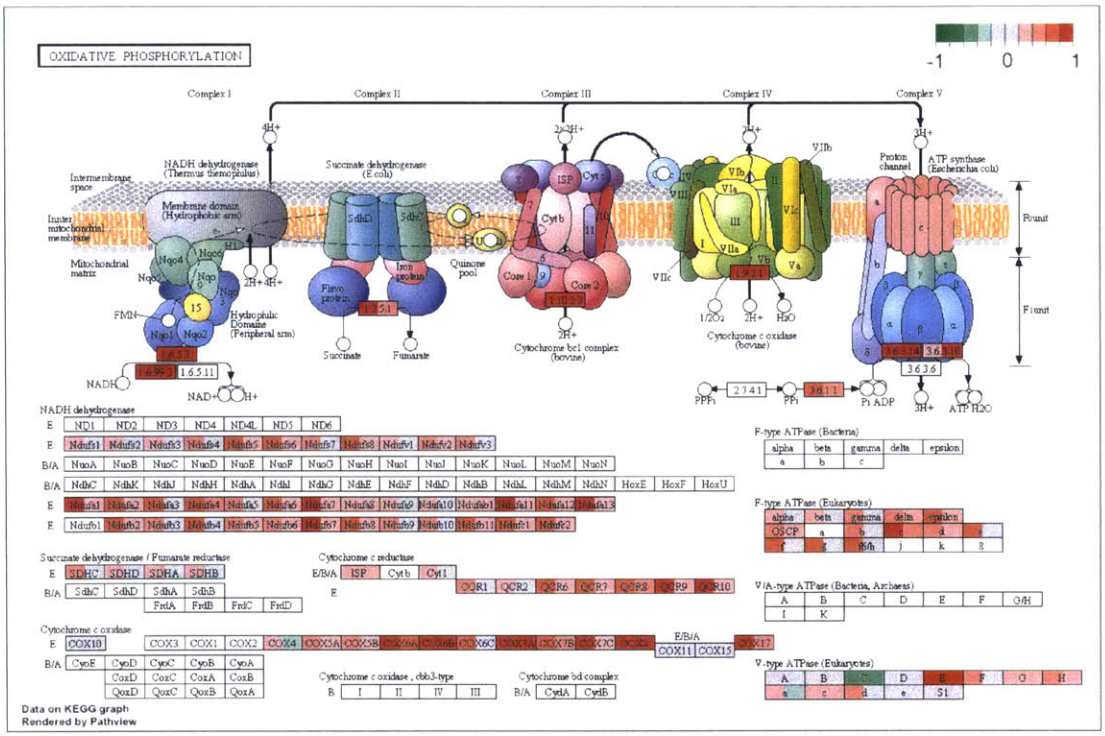

Figure 5: KEGG Oxidative phosphorylation pathway is significantly up-regulated in nGLT-1 KO (KO; N = 2) vs. WT littermate control (WT; N = 3) CA3 samples (t = 4.673; q = $2.80*10^{-8}$; set size = 117). Each gene/gene group indicates the relative expression of each nGLT-1 KO replicate to the mean expression level of all WT replicates. Red = increase in nGLT-1 gene expression; Green = decrease in nGLT-1 gene expression; color intensity indicates the relative change.

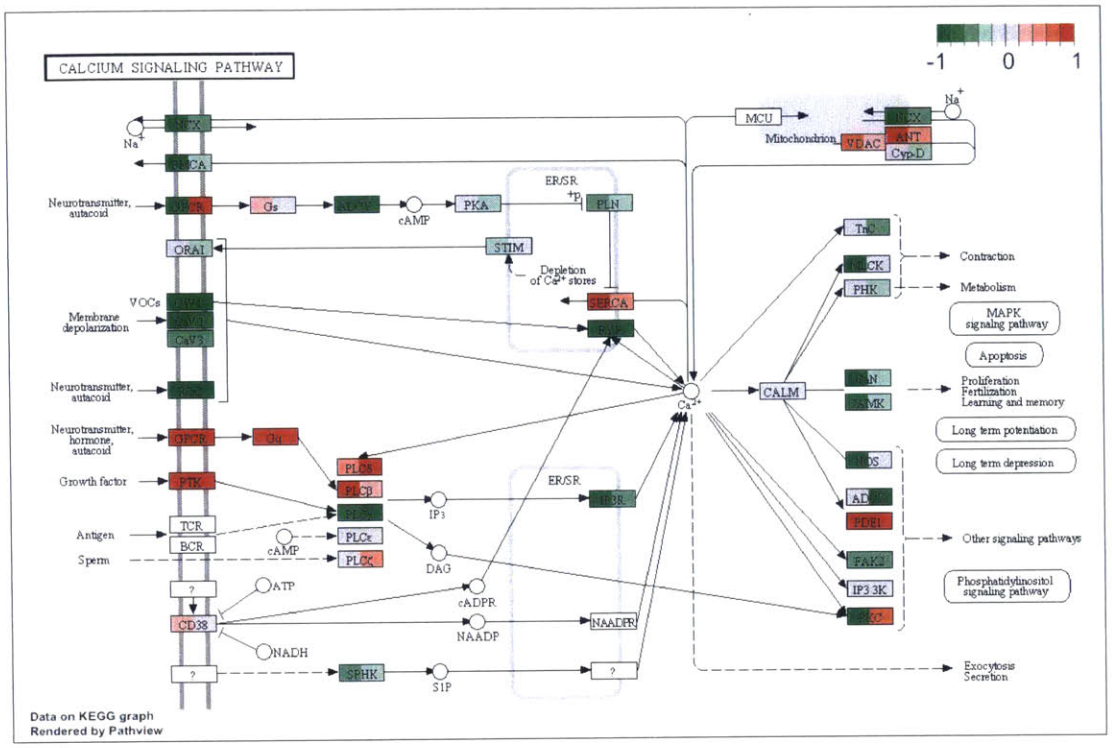

Figure 6: KEGG calcium signaling pathways is significantly altered in nGLT-1 KO (KO; N = 2) vs. WT littermate control (WT; N = 3) CA3 samples (t = 2.784; q = $3.18*10^{-3}$; set size = 178). Each gene/gene group indicates the relative expression of each nGLT-1 KO replicate to the mean expression level of all WT replicates. Red = increase in nGLT-1 gene expression; Green = decrease in nGLT-1 gene expression; color intensity indicates the relative change.

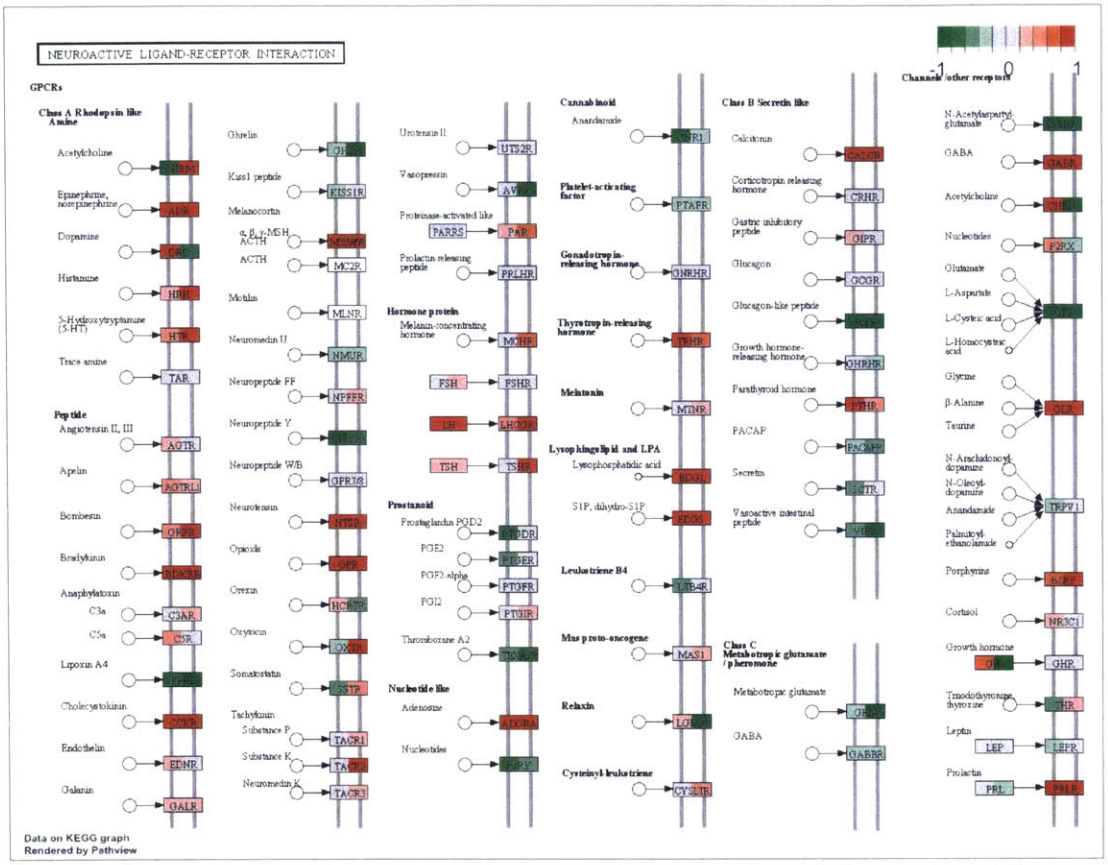

Figure 7: KEGG neuroactive ligand-receptor interaction pathway is significantly altered in nGLT-1 KO (KO; N = 2) vs. WT littermate control (WT; N = 3) CA3 samples ($t = 4.051$; $q = 1.46*10^{-6}$; set size = 260). Each gene/gene group indicates the relative expression of each nGLT-1 KO replicate to the mean expression level of all WT replicates. Red = increase in nGLT-1 gene expression; Green = decrease in nGLT-1 gene expression; color intensity indicates the relative change.

CA1

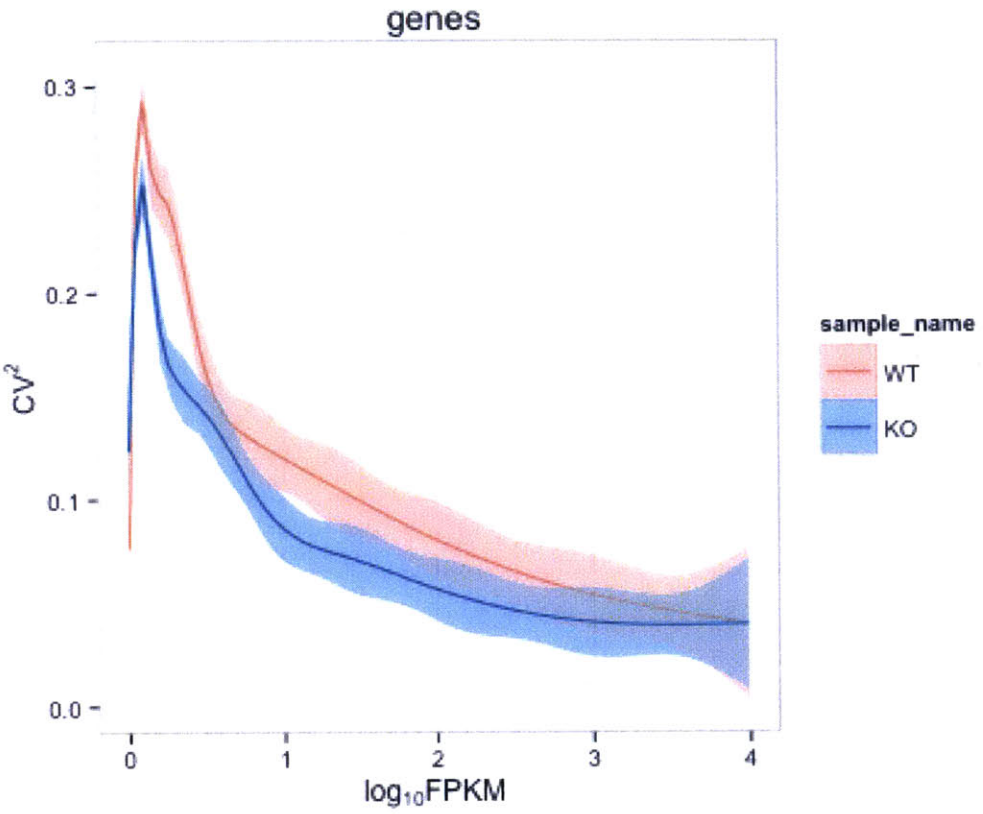

Figure 8: Variance analyses comparing CV^2 vs. $\log_{10}$FPKM values for all identified genes in nGLT-1 KO (KO; N = 2) and WT littermate control (WT; N = 3) CA1 samples. Differences in CV^2 vs. $\log_{10}$FPKM values were found for genes with adjusted transcript estimations between 0.0-0.6 $\log_{10}$FPKM; no differences in CV^2 vs. $\log_{10}$FPKM values were found for genes with adjusted transcript estimations > 0.6 $\log_{10}$FPKM. CV^2 = squared coefficient of variance; FPKM = fragments per kilobase of transcript per million mapped reads.

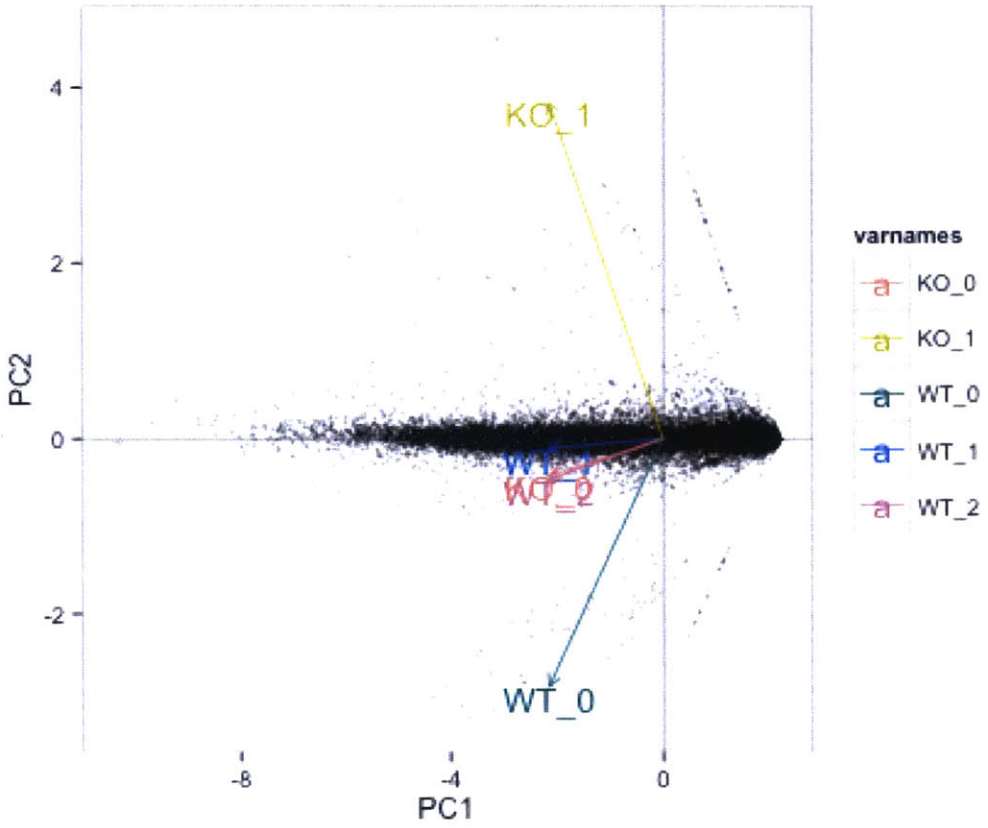

Figure 9: Principal Component Analysis comparing clustering of replicates over all identified genes in nGLT-1 KO (KO_0, KO_1) and WT littermate control (WT_0, WT_1, WT_2) CA1 samples. Distinct segregation of clustering was observed between KO_1 and WT replicates, however, KO_0 clustered with WT_1 and WT_2. PC1 = Principal Component 1; PC2 = Principal Component 2.

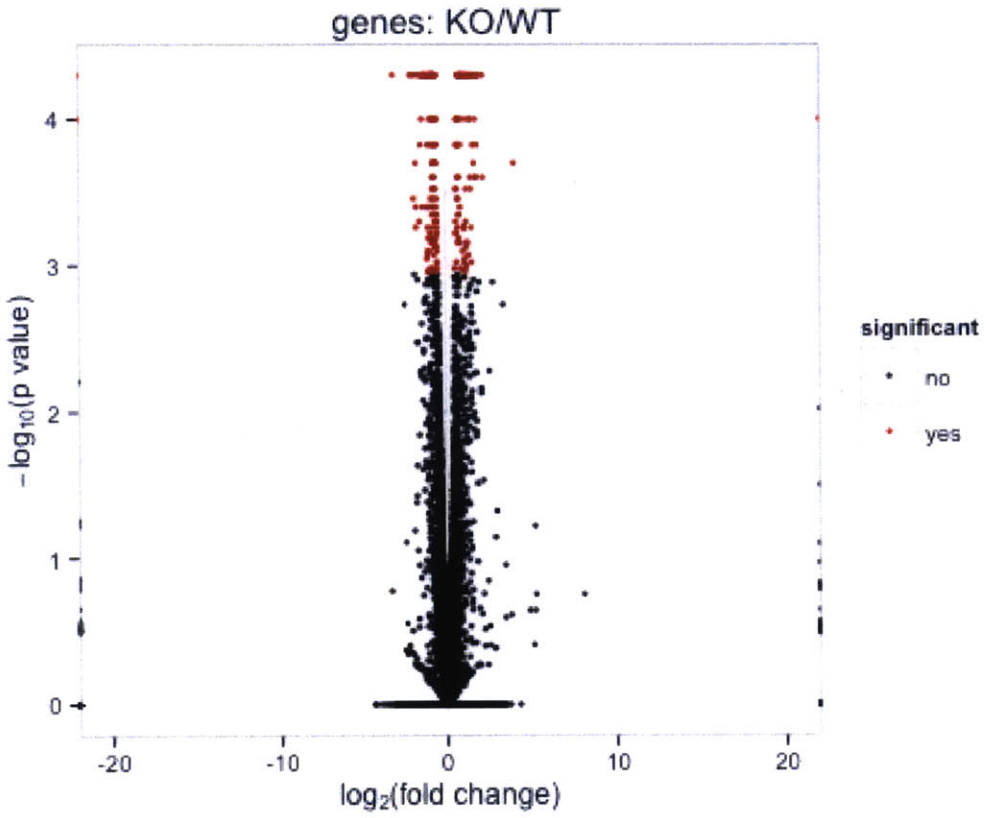

Figure 10: Volcano plot visualization of $-\log_{10}$(p-value) vs. $\log_2$(fold change in expression) for all identified genes in nGLT-1 KO (KO; N = 2) and WT littermate control (WT; N = 3) CA1 samples. Cuffdiff analysis revealed 322 differentially expressed genes ($q < 0.05$). Significant genes are indicated in red and non-significant genes are indicated in black. P-values correspond to the original, uncorrected statistical value; fold change corresponds to the KO/WT ratio of mean expression values for a given gene.

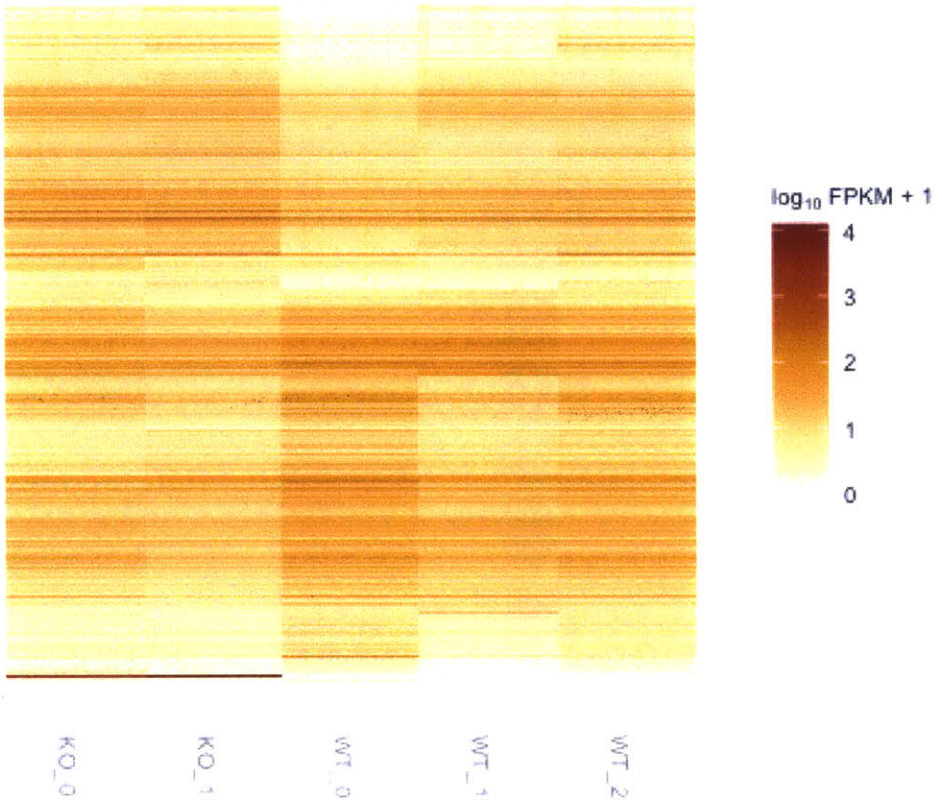

Figure 11: Heat map visualization of FPKM values for all replicates for all differentially regulated genes in nGLT-1 KO (KO_0, KO_1) and WT littermate control (WT_0, WT_1, WT_2) CA1 samples. Cuffdiff analysis revealed 322 differentially expressed genes ($q < 0.05$). FPKM = fragments per kilobase of transcript per million mapped reads.

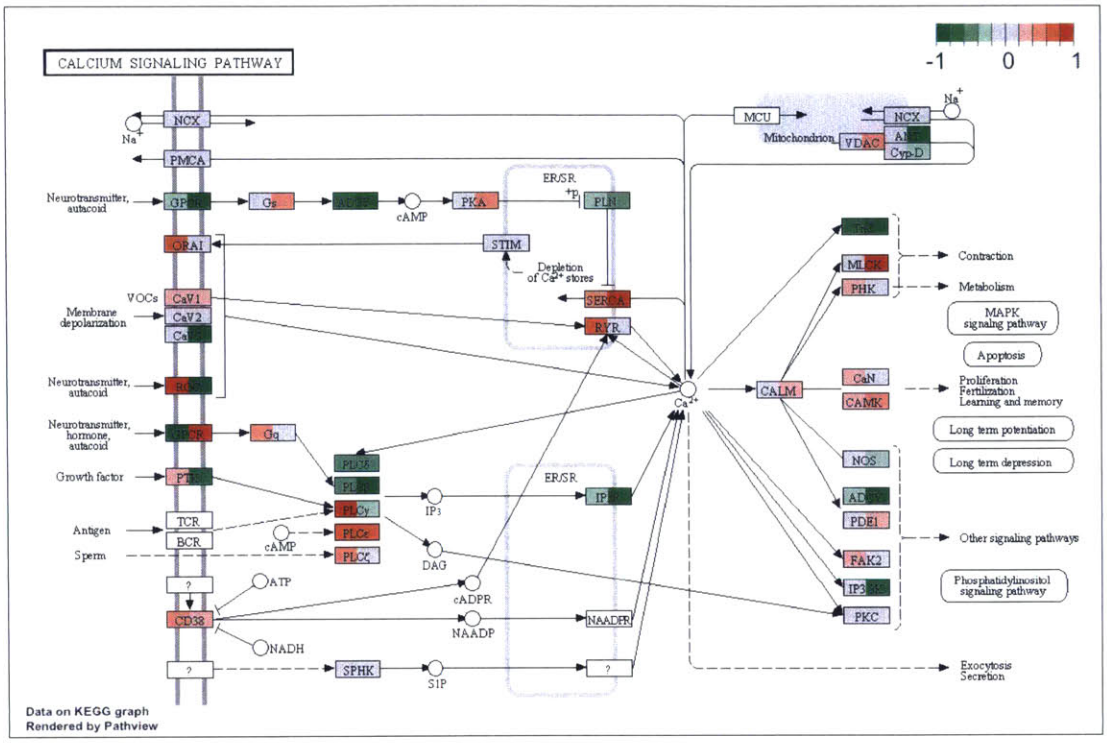

Figure 12: KEGG calcium signaling pathways is significantly altered in nGLT-1 KO (KO; N = 2) vs. WT littermate control (WT; N = 3) CA1 samples (t = 2.598; q = $6.84*10^{-3}$; set size = 178). Each gene/gene group indicates the relative expression of each nGLT-1 KO replicate to the mean expression level of all WT replicates. Red = increase in nGLT-1 gene expression; Green = decrease in nGLT-1 gene expression; color intensity indicates the relative change.

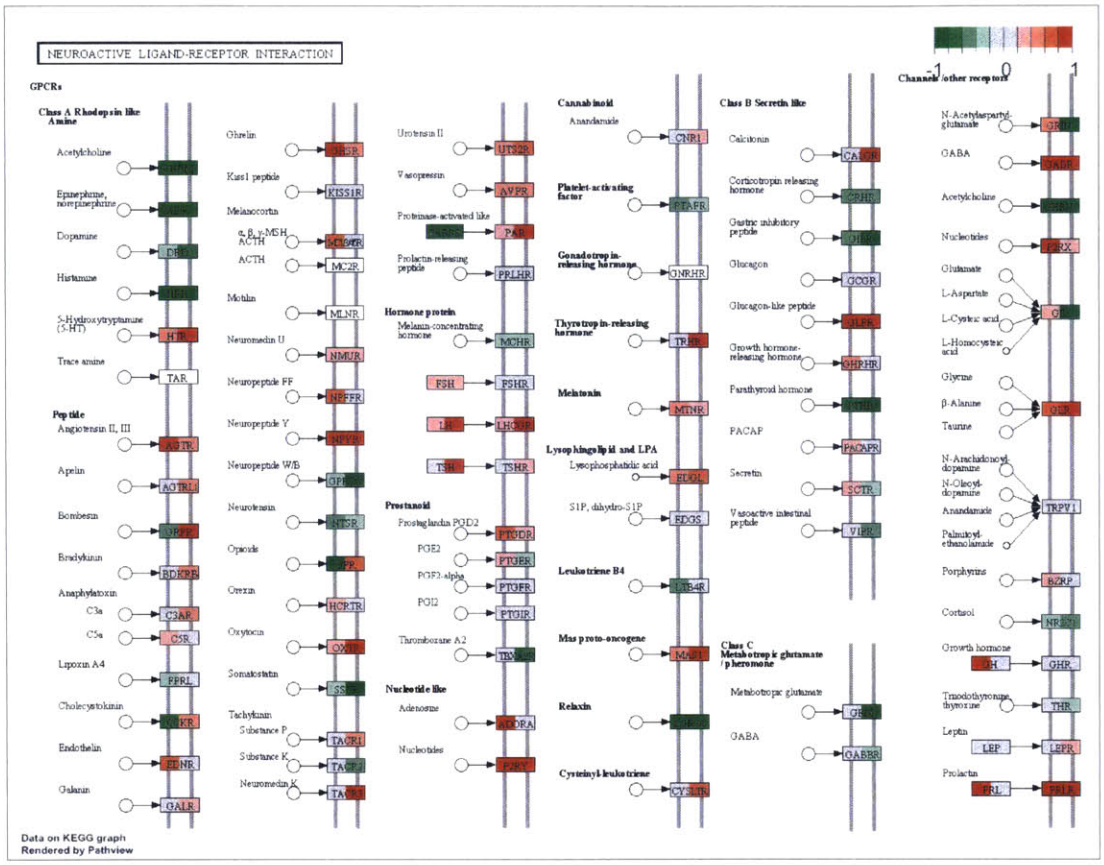

Figure 13: KEGG neuroactive ligand-receptor interaction pathway is significantly altered in nGLT-1 KO (KO; N = 2) vs. WT littermate control (WT; N = 3) CA1 samples ($t = 4.436$; $q = 6.15*10^{-8}$; set size = 255). Each gene/gene group indicates the relative expression of each nGLT-1 KO replicate to the mean expression level of all WT replicates. Red = increase in nGLT-1 gene expression; Green = decrease in nGLT-1 gene expression; color intensity indicates the relative change.

Striatum

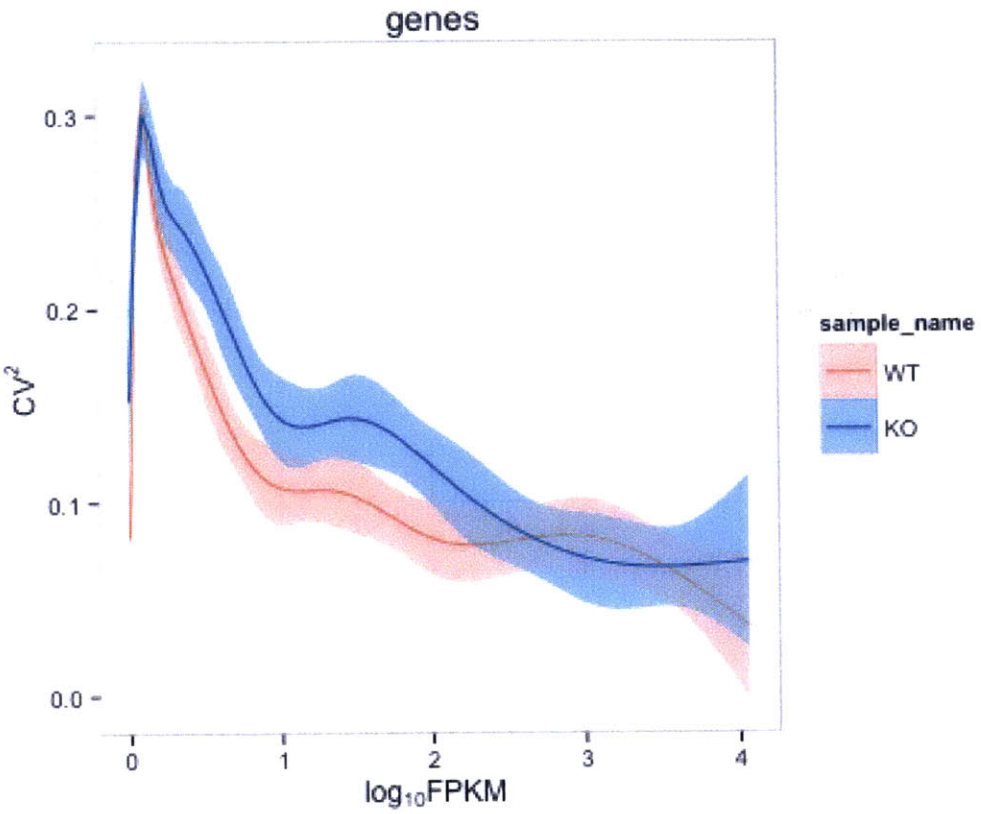

Figure 14: Variance analyses comparing CV^2 vs. $log_{10}FPKM$ values for all identified genes in nGLT-1 KO (KO; N = 2) and WT littermate control (WT; N = 3) Striatum samples. No differences in CV^2 vs. $log_{10}FPKM$ values were found. CV^2 = squared coefficient of variance; FPKM = fragments per kilobase of transcript per million mapped reads.

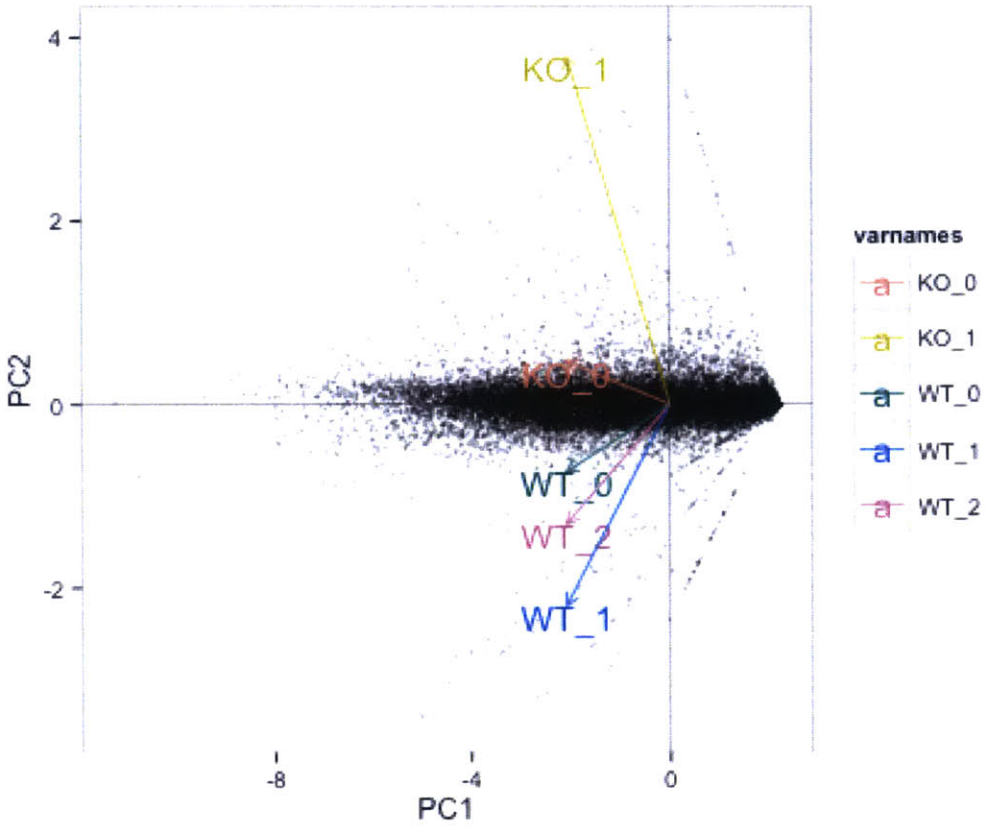

Figure 15: Principal Component Analysis comparing clustering of replicates over all identified genes in nGLT-1 KO (KO_0, KO_1) and WT littermate control (WT_0, WT_1, WT_2) Striatum samples. Distinct segregation of clustering was observed between nGLT-1 KO and WT replicates; however, a significant distance between KO_0 and KO_1 was observed. PC1 = Principal Component 1; PC2 = Principal Component 2.

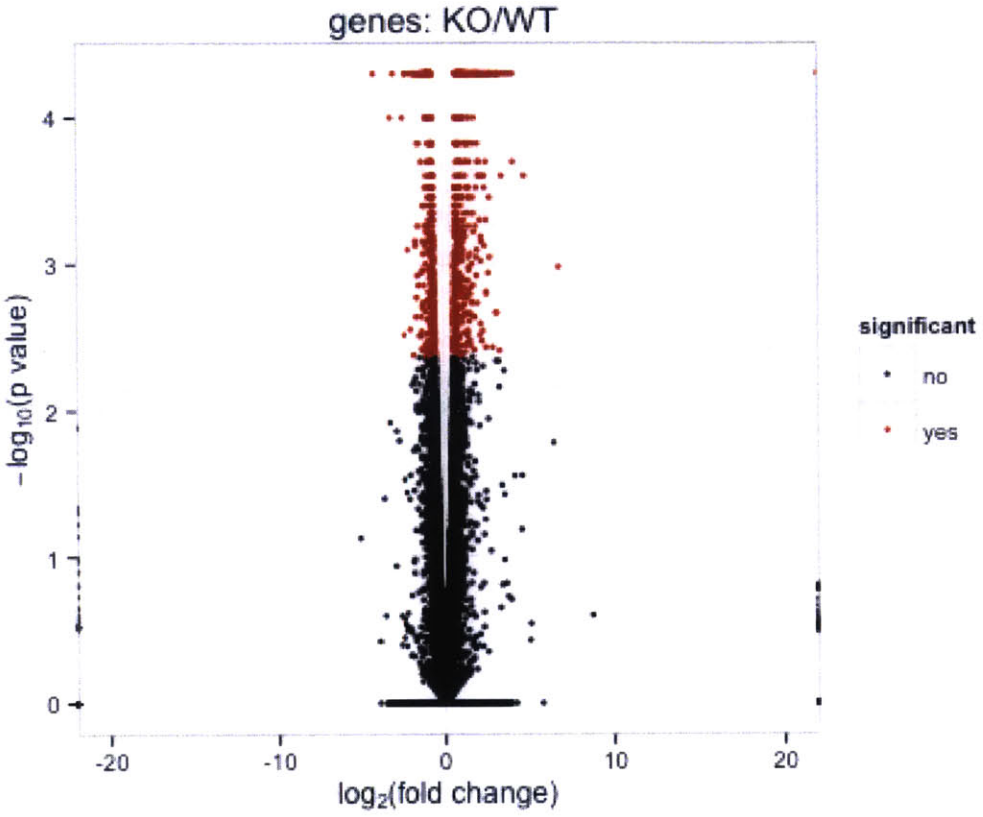

Figure 16: Volcano plot visualization of $-\log_{10}$(p-value) vs. $\log_2$(fold change in expression) for all identified genes in nGLT-1 KO (KO; N = 2) and WT littermate control (WT; N = 3) Striatum samples. Cuffdiff analysis revealed 1268 differentially expressed genes ($q < 0.05$). Significant genes are indicated in red and non-significant genes are indicated in black. P-values correspond to the original, uncorrected statistical value; fold change corresponds to the KO/WT ratio of mean expression values for a given gene.

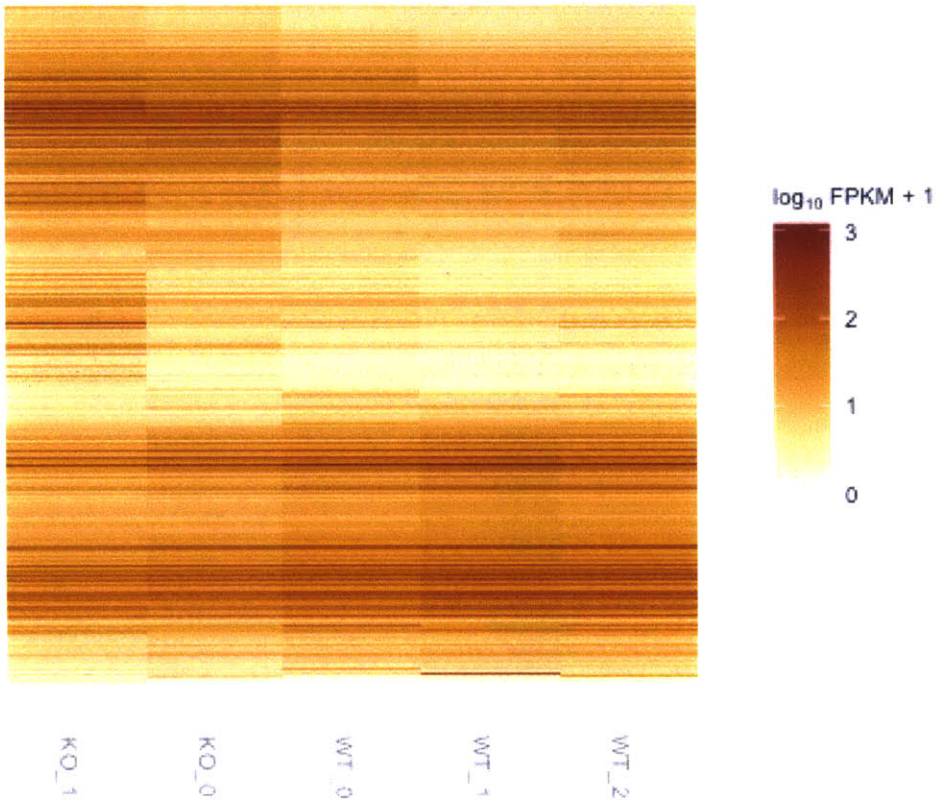

Figure 17: Heat map visualization of FPKM values for all replicates for all differentially regulated genes in nGLT-1 KO (KO_0, KO_1) and WT littermate control (WT_0, WT_1, WT_2) Striatum samples. Cuffdiff analysis revealed 1268 differentially expressed genes ($q < 0.05$). FPKM = fragments per kilobase of transcript per million mapped reads.

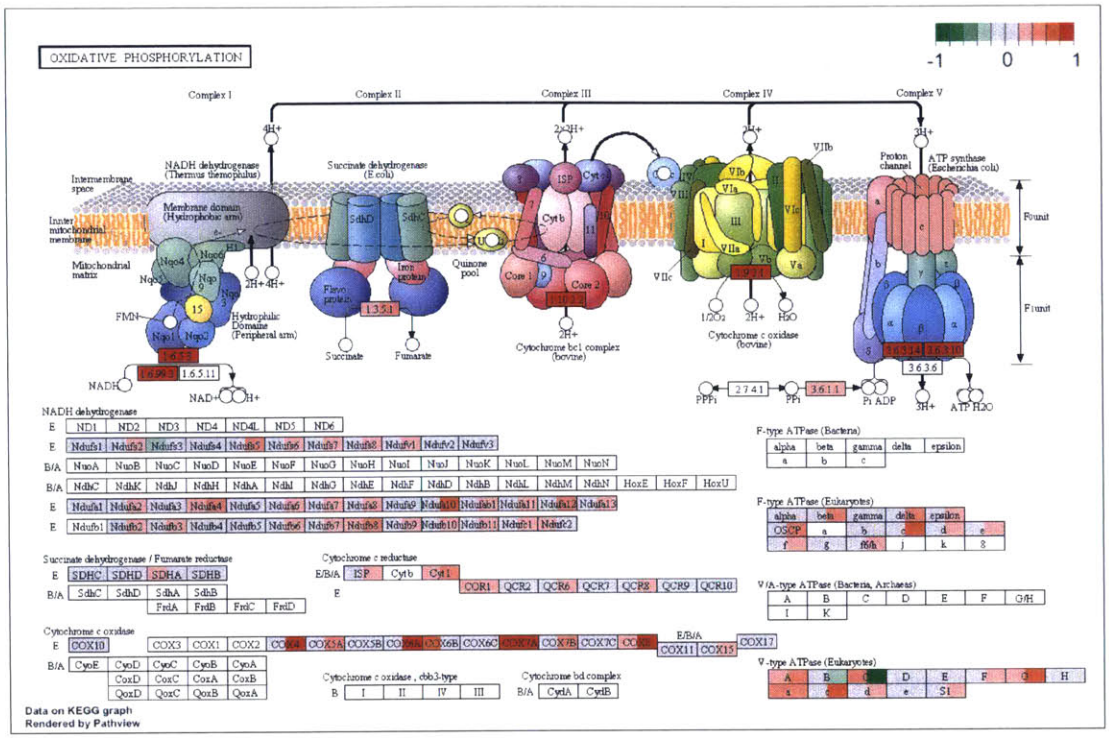

Figure 18: KEGG Oxidative phosphorylation pathway is significantly up-regulated in nGLT-1 KO (KO; N = 2) vs. WT littermate control (WT; N = 3) Striatum samples (t = 1.999; q = $9.65*10^{-2}$; set size = 117). Each gene/gene group indicates the relative expression of each nGLT-1 KO replicate to the mean expression level of all WT replicates. Red = increase in nGLT-1 gene expression; Green = decrease in nGLT-1 gene expression; color intensity indicates the relative change.

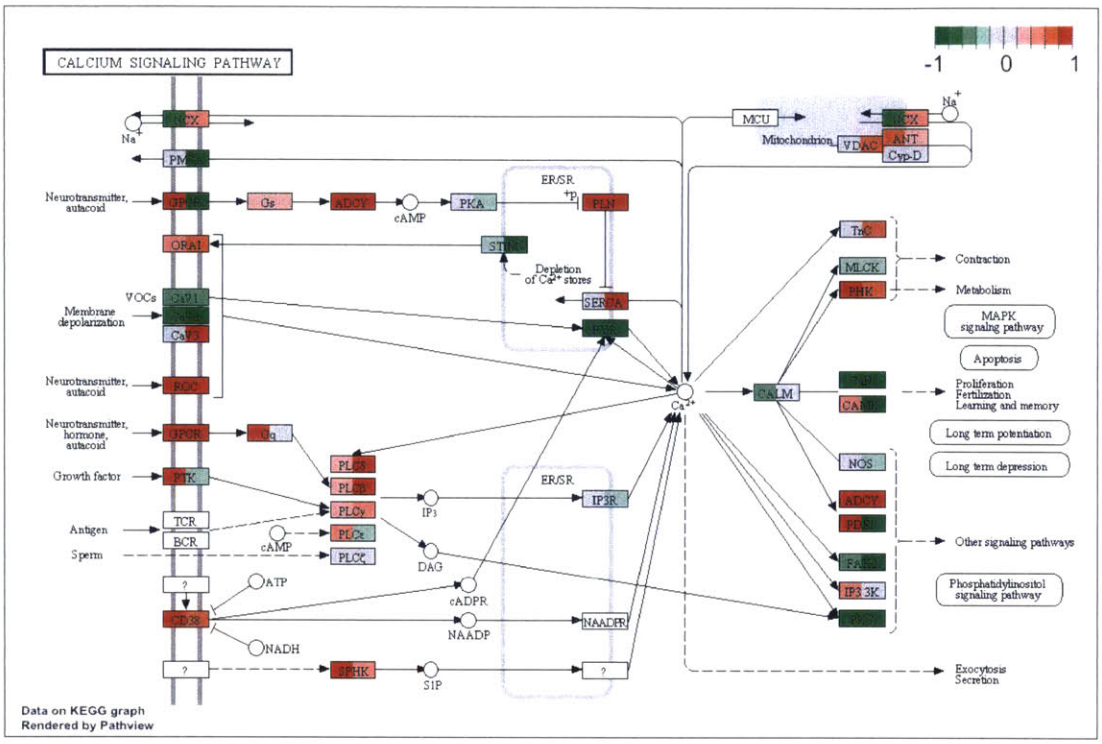

Figure 19: KEGG calcium signaling pathways is significantly altered in nGLT-1 KO (KO; N = 2) vs. WT littermate control (WT; N = 3) Striatum samples (t = 4.309; q = $1.14*10^{-7}$; set size = 178). Each gene/gene group indicates the relative expression of each nGLT-1 KO replicate to the mean expression level of all WT replicates. Red = increase in nGLT-1 gene expression; Green = decrease in nGLT-1 gene expression; color intensity indicates the relative change.

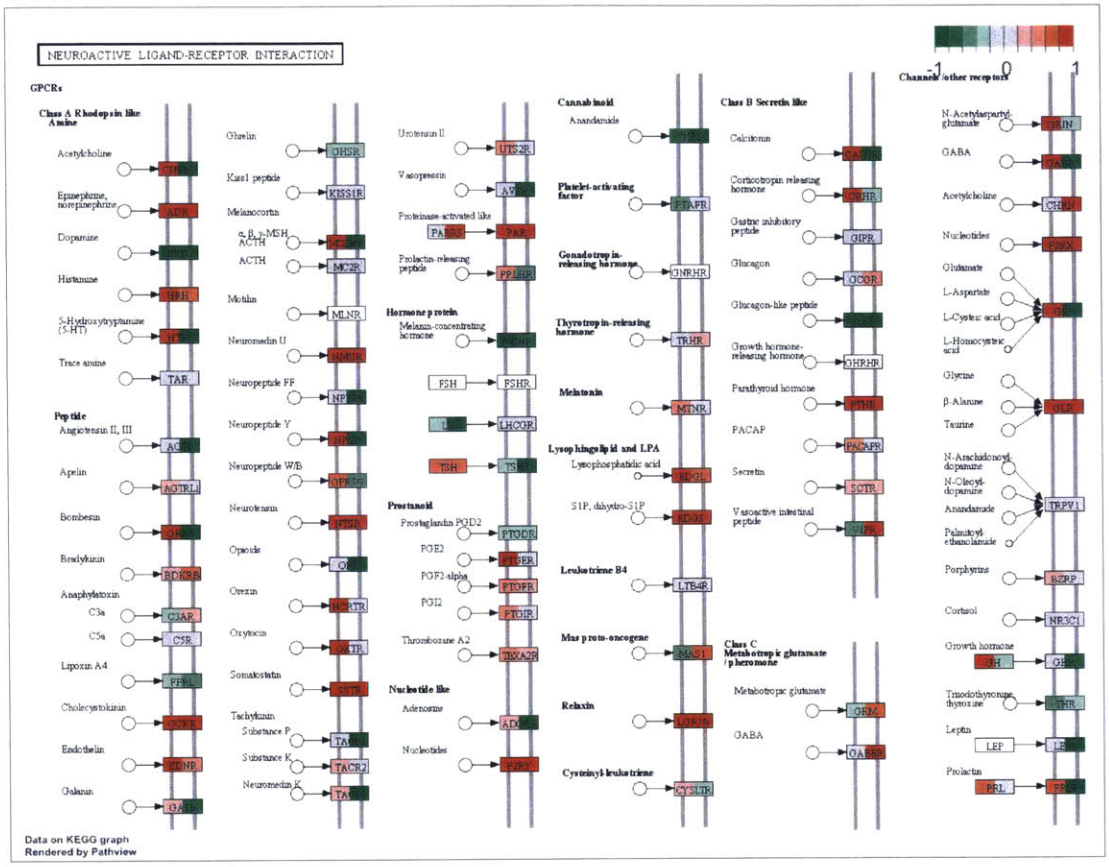

Figure 20: KEGG neuroactive ligand-receptor interaction pathway is significantly altered in nGLT-1 KO (KO; N = 2) vs. WT littermate control (WT; N = 3) Striatum samples (t = 5.789; q = $1.22*10^{-13}$; set size = 251). Each gene/gene group indicates the relative expression of each nGLT-1 KO replicate to the mean expression level of all WT replicates. Red = increase in nGLT-1 gene expression; Green = decrease in nGLT-1 gene expression; color intensity indicates the relative change.

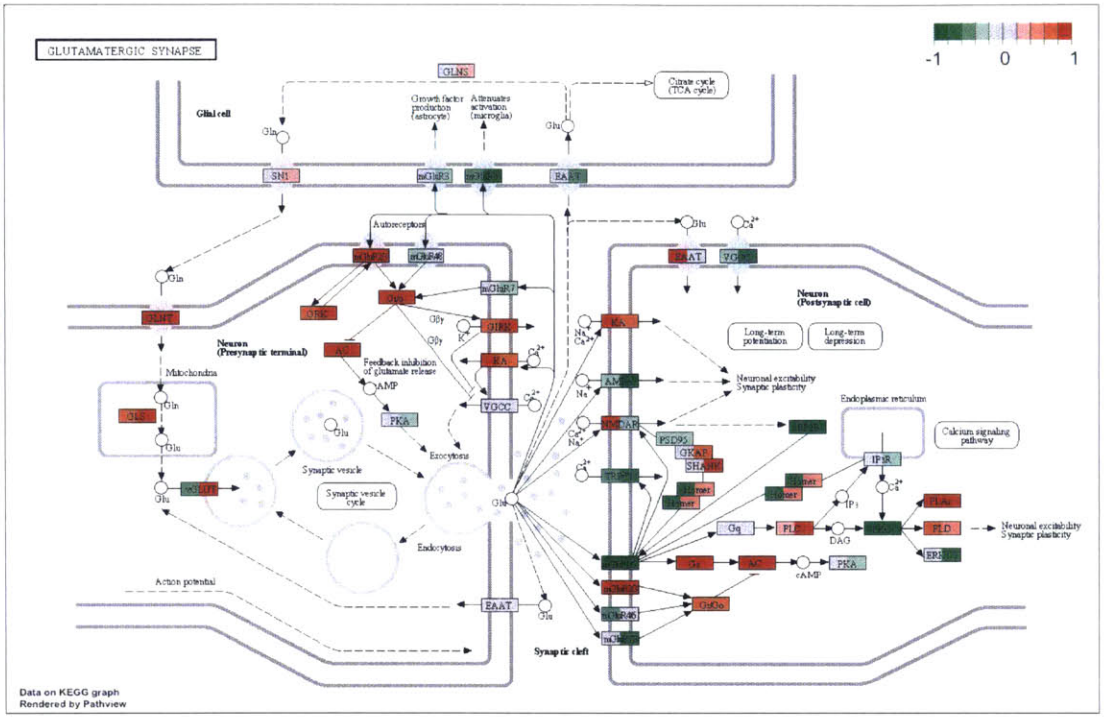

Figure 21: KEGG glutamatergic synapse pathway is significantly altered in nGLT-1 KO (KO; N = 2) vs. WT littermate control (WT; N = 3) Striatum samples (t = 3.302; q = $9.66*10^{-5}$; set size = 111). Each gene/gene group indicates the relative expression of each nGLT-1 KO replicate to the mean expression level of all WT replicates. Red = increase in nGLT-1 gene expression; Green = decrease in nGLT-1 gene expression; color intensity indicates the relative change.

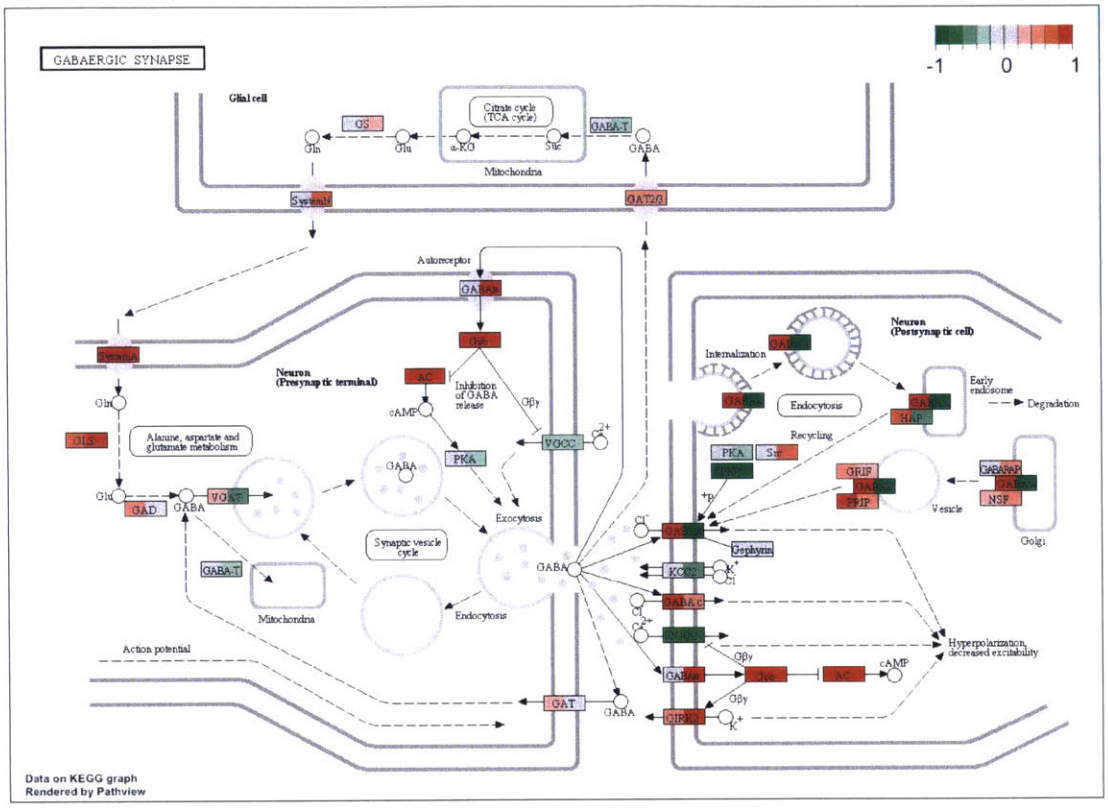

Figure 22: KEGG GABAergic synapse pathway is significantly altered in nGLT-1 KO (KO; N = 2) vs. WT littermate control (WT; N = 3) Striatum samples (t = 2.200; q = $9.27*10^{-3}$; set size = 87). Each gene/gene group indicates the relative expression of each nGLT-1 KO replicate to the mean expression level of all WT replicates. Red = increase in nGLT-1 gene expression; Green = decrease in nGLT-1 gene expression; color intensity indicates the relative change.

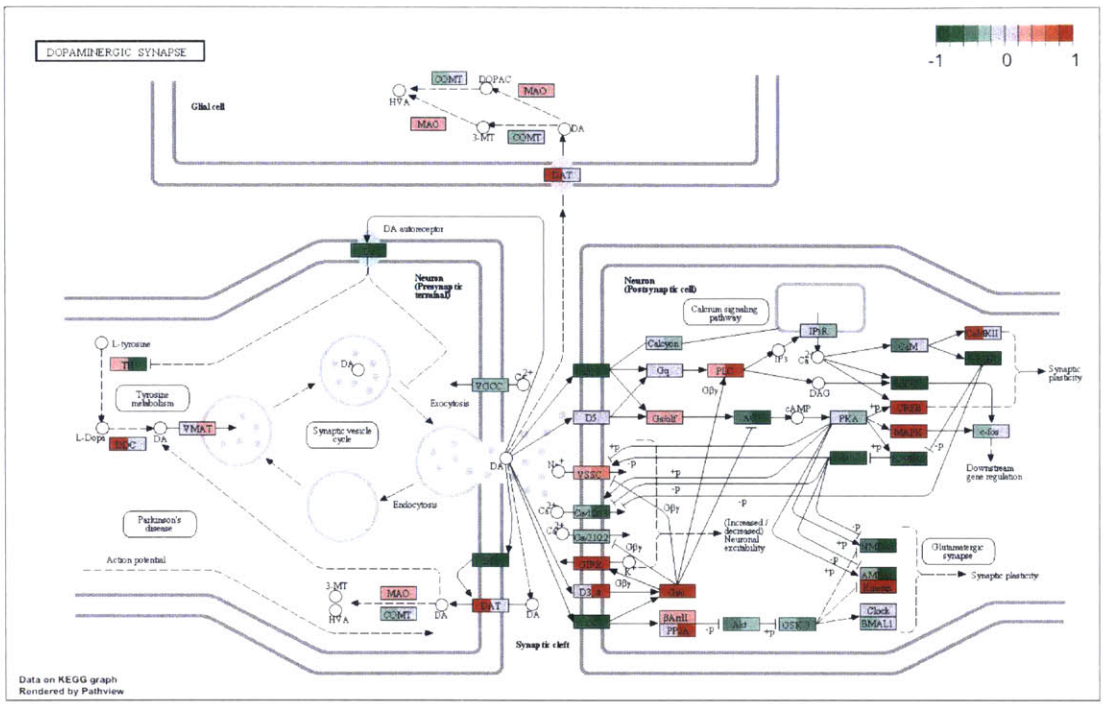

Figure 23: KEGG dopaminergic synapse pathway is significantly altered in nGLT-1 KO (KO; N = 2) vs. WT littermate control (WT; N = 3) Striatum samples (t = 1.888; q = $2.89*10^{-2}$; set size = 127). Each gene/gene group indicates the relative expression of each nGLT-1 KO replicate to the mean expression level of all WT replicates. Red = increase in nGLT-1 gene expression; Green = decrease in nGLT-1 gene expression; color intensity indicates the relative change.

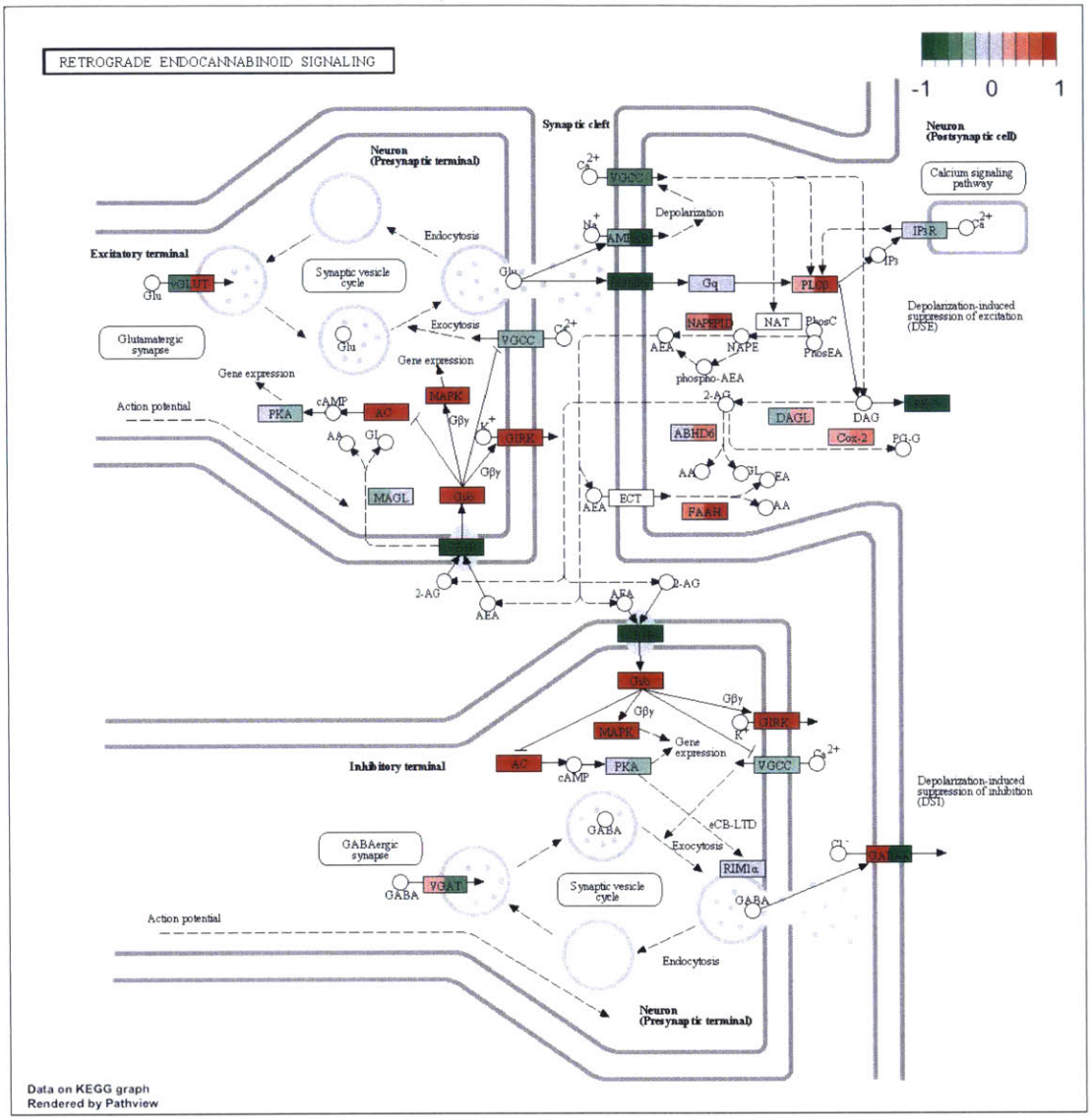

Figure 24: KEGG retrograde endocannabinoid signaling pathway is significantly altered in nGLT-1 KO (KO; N = 2) vs. WT littermate control (WT; N = 3) Striatum samples (t = 3.263; q = $1.10*10^{-4}$; set size = 101). Each gene/gene group indicates the relative expression of each nGLT-1 KO replicate to the mean expression level of all WT replicates. Red = increase in nGLT-1 gene expression; Green = decrease in nGLT-1 gene expression; color intensity indicates the relative change.

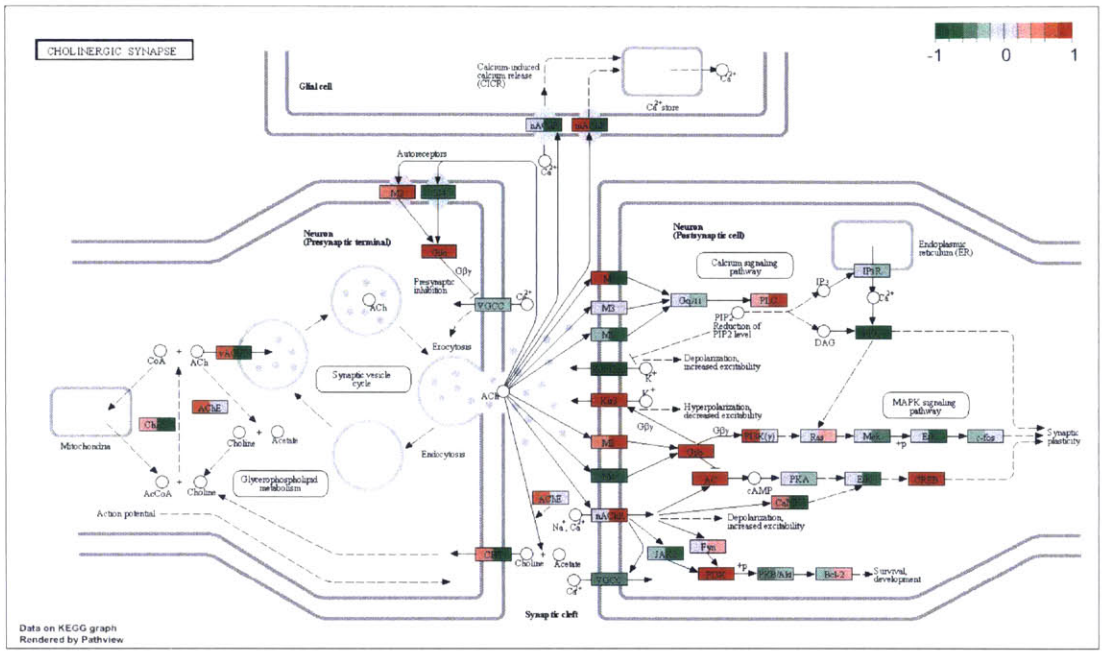

Figure 25: KEGG cholinergic synapse pathway is significantly altered in nGLT-1 KO (KO; N = 2) vs. WT littermate control (WT; N = 3) Striatum samples (t = 2.710; q = $1.82*10^{-3}$; set size = 112). Each gene/gene group indicates the relative expression of each nGLT-1 KO replicate to the mean expression level of all WT replicates. Red = increase in nGLT-1 gene expression; Green = decrease in nGLT-1 gene expression; color intensity indicates the relative change.

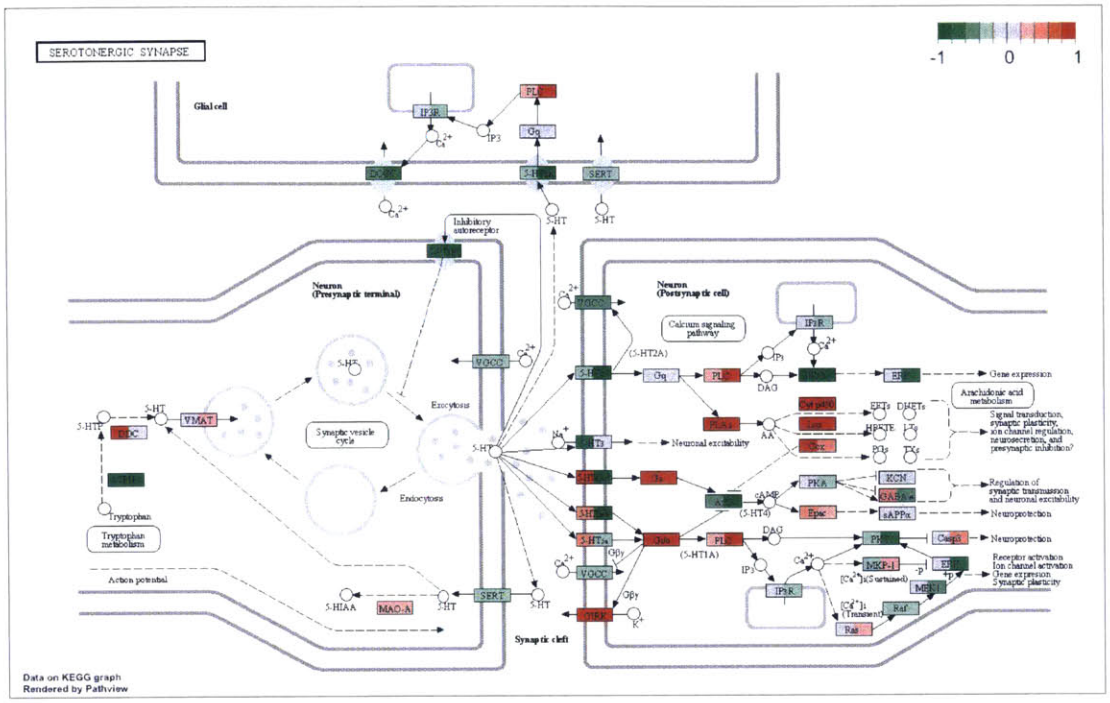

Figure 26: KEGG serotonergic synapse pathway is significantly altered in nGLT-1 KO (KO; N = 2) vs. WT littermate control (WT; N = 3) Striatum samples (t = 2.649; q = $1.99*10^{-3}$; set size = 119). Each gene/gene group indicates the relative expression of each nGLT-1 KO replicate to the mean expression level of all WT replicates. Red = increase in nGLT-1 gene expression; Green = decrease in nGLT-1 gene expression; color intensity indicates the relative change.

References

Baker DA, Xi ZX, Shen H, Swanson CJ, Kalivas PW (2002) The origin and neuronal function of in vivo nonsynaptic glutamate. J Neurosci 22:9134–9141.

Balcar VJ, Johnston GA (1972) The structural specificity of the high affinity uptake of L-glutamate and L-aspartate by rat brain slices. J Neurochem 19:2657–2666 Available at: http://www.ncbi.nlm.nih.gov/pubmed/4404455 [Accessed August 20, 2015].

Bellesi M, Conti F (2010) The mGluR2/3 agonist LY379268 blocks the effects of GLT-1 upregulation on prepulse inhibition of the startle reflex in adult rats. Neuropsychopharmacology 35:1253–1260.

Bennett BD, Bolam JP (1994) Synaptic input and output of parvalbumin-immunoreactive neurons in the neostriatum of the rat. Neuroscience 62:707–719 Available at: http://www.ncbi.nlm.nih.gov/pubmed/7870301 [Accessed July 7, 2015].

Berger U V, DeSilva TM, Chen W, Rosenberg PA (2005a) Cellular and subcellular mRNA localization of glutamate transporter isoforms GLT1a and GLT1b in rat brain by in situ hybridization. J Comp Neurol 492:78–89.

Berger U V, DeSilva TM, Chen W, Rosenberg PA (2005b) Cellular and subcellular mRNA localization of glutamate transporter isoforms GLT1a and GLT1b in rat brain by in situ hybridization. J Comp Neurol 492:78–89 Available at: http://www.pubmedcentral.nih.gov/articlerender.fcgi?artid=3676901&tool=pmcentrez&rendertype=abstract [Accessed April 18, 2014].

Berger U V, Hediger M a (1998) Comparative analysis of glutamate transporter expression in rat brain using differential double in situ hybridization. Anat Embryol (Berl) 198:13–30 Available at: http://www.ncbi.nlm.nih.gov/pubmed/9683064.

Berke JD (2011) Functional properties of striatal fast-spiking interneurons. Front Syst Neurosci 5:45 Available at: http://www.pubmedcentral.nih.gov/articlerender.fcgi?artid=3121016&tool=pmcentrez&rendertype=abstract [Accessed August 23, 2015].

Berridge MJ (1998) Neuronal calcium signaling. Neuron 21:13–26 Available at: http://www.ncbi.nlm.nih.gov/pubmed/9697848 [Accessed June 18, 2015].

Bickerdike MJ, Abercrombie ED (1997) Striatal acetylcholine release correlates with behavioral sensitization in rats withdrawn from chronic amphetamine. J Pharmacol Exp Ther 282:818–826 Available at: http://www.ncbi.nlm.nih.gov/pubmed/9262346 [Accessed August 23, 2015].

Blandini F, Porter RH, Greenamyre JT (1996) Glutamate and Parkinson's disease. Mol Neurobiol 12:73–94 Available at: http://www.ncbi.nlm.nih.gov/pubmed/8732541 [Accessed April 18, 2014].

Bowers MS, Chen BT, Bonci A (2010) AMPA receptor synaptic plasticity induced by psychostimulants: the past, present, and therapeutic future. Neuron 67:11–24 Available at: http://www.pubmedcentral.nih.gov/articlerender.fcgi?artid=2904302&tool=pmcentrez&rendertype=abstract [Accessed August 23, 2015].

Burns LH, Everitt BJ, Kelley AE, Robbins TW (1994) Glutamate-dopamine interactions in the ventral striatum: role in locomotor activity and responding with conditioned reinforcement. Psychopharmacology (Berl) 115:516–528 Available at: http://www.ncbi.nlm.nih.gov/pubmed/7871097 [Accessed August 23, 2015].

Cedillo LN, Miranda F (2013) Effects of co-administration of the GABAB receptor agonist baclofen and a positive allosteric modulator of the GABAB receptor, CGP7930, on the development and expression of amphetamine-induced locomotor sensitization in rats. Pharmacol Rep 65:1132–1143 Available at: http://www.ncbi.nlm.nih.gov/pubmed/24399709 [Accessed August 23, 2015].

Chen W, Aoki C, Mahadomrongkul V, Gruber CE, Wang GJ, Blitzblau R, Irwin N, Rosenberg PA (2002) Expression of a variant form of the glutamate transporter GLT1 in neuronal cultures and in neurons and astrocytes in the rat brain. J Neurosci 22:2142–2152 Available at: http://www.pubmedcentral.nih.gov/articlerender.fcgi?artid=2849837&tool=pmcentrez&rendertype=abstract [Accessed April 18, 2014].

Chen W, Mahadomrongkul V, Berger U V, Bassan M, DeSilva T, Tanaka K, Irwin N, Aoki C, Rosenberg PA (2004) The glutamate transporter GLT1a is expressed in excitatory axon terminals of mature hippocampal neurons. J Neurosci 24:1136–1148.

Chesselet M-F, Plotkin JL, Wu N, Levine MS (2007) Development of striatal fast-spiking GABAergic interneurons. Prog Brain Res 160:261–272 Available at: http://www.ncbi.nlm.nih.gov/pubmed/17499119 [Accessed August 23, 2015].

Clapham DE (2007) Calcium signaling. Cell 131:1047–1058 Available at: http://www.cell.com/article/S0092867407015310/fulltext [Accessed July 11, 2014].

Cousin MA, Robinson PJ (1999) Mechanisms of synaptic vesicle recycling illuminated by fluorescent dyes. J Neurochem 73:2227–2239 Available at: http://www.ncbi.nlm.nih.gov/pubmed/10582580 [Accessed August 20, 2015].

Danbolt NC (2001) Glutamate uptake. Prog Neurobiol 65:1–105 Available at: http://www.ncbi.nlm.nih.gov/pubmed/11369436 [Accessed April 7, 2014].

David HN, Abraini JH (2003) Blockade of the locomotor stimulant effects of amphetamine by group I, group II, and group III metabotropic glutamate receptor ligands in the rat nucleus accumbens: possible interactions with dopamine receptors. Neuropharmacology 44:717–727 Available at: http://www.ncbi.nlm.nih.gov/pubmed/12681370 [Accessed August 23, 2015].

Dong X, Wang Y, Qin Z (2009) Molecular mechanisms of excitotoxicity and their relevance to pathogenesis of neurodegenerative diseases. Acta Pharmacol Sin 30:379–387 Available at: http://dx.doi.org/10.1038/aps.2009.24 [Accessed March 11, 2015].

Finsterer J, Jarius C, Baumgartner M (2001) Parkinson's disease associated with impaired oxidative phosphorylation. Neuroradiology 43:997–1000 Available at: http://www.ncbi.nlm.nih.gov/pubmed/11760809 [Accessed August 23, 2015].

Fischer K, Houston A, Desai R, Doyle M, Bergman J, Mian M, Rosenberg P (2015) Conditional deletion of the glutamate transporter GLT-1 in neurons attenuates amphetamine-induced behavioral activation. Prep J Neurosci.

Fischer KD, Houston ACW, Rebec G V (2013) Role of the major glutamate transporter GLT1 in nucleus accumbens core versus shell in cue-induced cocaine-seeking behavior. J Neurosci 33:9319–9327 Available at: http://www.pubmedcentral.nih.gov/articlerender.fcgi?artid=3694387&tool=pmcentrez&rendertype=abstract [Accessed August 23, 2015].

Fonnum F (1984) Glutamate: a neurotransmitter in mammalian brain. J Neurochem 42:1–11 Available at: http://www.ncbi.nlm.nih.gov/pubmed/6139418 [Accessed August 18, 2015].

Furness DN, Dehnes Y, Akhtar AQ, Rossi DJ, Hamann M, Grutle NJ, Gundersen V, Holmseth S, Lehre KP, Ullensvang K, Wojewodzic M, Zhou Y, Attwell D, Danbolt NC (2008) A quantitative assessment of glutamate uptake into hippocampal synaptic terminals and astrocytes: new insights into a neuronal role for excitatory amino acid transporter 2 (EAAT2). Neuroscience 157:80–94 Available at: http://www.pubmedcentral.nih.gov/articlerender.fcgi?artid=2775085&tool=pmcentrez&rendertype=abstract [Accessed April 18, 2014].

Genda EN, Jackson JG, Sheldon AL, Locke SF, Greco TM, O'Donnell JC, Spruce LA, Xiao R, Guo W, Putt M, Seeholzer S, Ischiropoulos H, Robinson MB (2011) Co-compartmentalization of the astroglial glutamate transporter, GLT-1, with glycolytic enzymes and mitochondria. J Neurosci 31:18275–18288 Available at: http://www.pubmedcentral.nih.gov/articlerender.fcgi?artid=3259858&tool=pmcentrez&rendertype=abstract [Accessed August 23, 2015].

Goecks J, Nekrutenko A, Taylor J (2010) Galaxy: a comprehensive approach for supporting accessible, reproducible, and transparent computational research in the life sciences. Genome Biol 11:R86 Available at: http://www.pubmedcentral.nih.gov/articlerender.fcgi?artid=2945788&tool=pmcentrez&rendertype=abstract [Accessed July 10, 2014].

Goff DC, Coyle JT (2001) The emerging role of glutamate in the pathophysiology and treatment of schizophrenia. Am J Psychiatry 158:1367–1377 Available at: http://www.ncbi.nlm.nih.gov/pubmed/11532718 [Accessed April 18, 2014].

Goursaud S, Maloteaux J-M, Hermans E (2008) Distinct expression and regulation of the glutamate transporter isoforms GLT-1a and GLT-1b in cultured astrocytes from a rat model of amyotrophic lateral sclerosis (hSOD1G93A). Neurochem Int 55:28–34 Available at: http://www.ncbi.nlm.nih.gov/pubmed/19428804 [Accessed August 20, 2015].

Hack N, Balázs R (1994) Selective stimulation of excitatory amino acid receptor subtypes and the survival of granule cells in culture: effect of quisqualate and AMPA. Neurochem Int 25:235–241 Available at: http://www.ncbi.nlm.nih.gov/pubmed/7530540 [Accessed August 20, 2015].

Haugeto O, Ullensvang K, Levy LM, Chaudhry FA, Honoré T, Nielsen M, Lehre KP, Danbolt NC (1996) Brain glutamate transporter proteins form homomultimers. J Biol Chem 271:27715–27722 Available at: http://www.ncbi.nlm.nih.gov/pubmed/8910364 [Accessed August 21, 2015].

Ishizuka N, Weber J, Amaral DG (1990) Organization of intrahippocampal projections originating from CA3 pyramidal cells in the rat. J Comp Neurol 295:580–623 Available at: http://www.ncbi.nlm.nih.gov/pubmed/2358523 [Accessed October 3, 2014].

Jackson JG, O'Donnell JC, Takano H, Coulter D a, Robinson MB (2014) Neuronal activity and glutamate uptake decrease mitochondrial mobility in astrocytes and position mitochondria near glutamate transporters. J Neurosci 34:1613–1624 Available at: http://www.pubmedcentral.nih.gov/articlerender.fcgi?artid=3905137&tool=pmcentrez&rendertype=abstract [Accessed October 12, 2014].

Katagiri H, Tanaka K, Manabe T (2001) Requirement of appropriate glutamate concentrations in the synaptic cleft for hippocampal LTP induction. Eur J Neurosci 14:547–553 Available at: http://www.ncbi.nlm.nih.gov/pubmed/11553304 [Accessed January 21, 2015].

Kim D, Pertea G, Trapnell C, Pimentel H, Kelley R, Salzberg SL (2013) TopHat2: accurate alignment of transcriptomes in the presence of insertions, deletions and gene fusions. Genome Biol 14:R36 Available at: http://genomebiology.com/2013/14/4/R36 [Accessed July 9, 2014].

Knackstedt LA, Melendez RI, Kalivas PW (2010) Ceftriaxone restores glutamate homeostasis and prevents relapse to cocaine seeking. Biol Psychiatry 67:81–84 Available at: http://www.pubmedcentral.nih.gov/articlerender.fcgi?artid=2795043&tool=pmcentrez&rendertype=abstract [Accessed August 21, 2015].

Knowles JR (1980) Enzyme-catalyzed phosphoryl transfer reactions. Annu Rev Biochem 49:877–919 Available at: http://www.ncbi.nlm.nih.gov/pubmed/6250450 [Accessed August 23, 2015].

Lehre KP, Danbolt NC (1998) The number of glutamate transporter subtype molecules at glutamatergic synapses: chemical and stereological quantification in young adult rat brain. J Neurosci 18:8751–8757 Available at: http://www.ncbi.nlm.nih.gov/pubmed/9786982 [Accessed August 23, 2015].

Levin JZ, Yassour M, Adiconis X, Nusbaum C, Thompson DA, Friedman N, Gnirke A, Regev A (2010) Comprehensive comparative analysis of strand-specific RNA sequencing methods. Nat Methods 7:709–715 Available at: http://www.pubmedcentral.nih.gov/articlerender.fcgi?artid=3005310&tool=pmcentrez&rendertype=abstract [Accessed March 17, 2015].

Levy LM, Warr O, Attwell D (1998) Stoichiometry of the Glial Glutamate Transporter GLT-1 Expressed Inducibly in a Chinese Hamster Ovary Cell Line Selected for Low Endogenous Na+-Dependent Glutamate Uptake. J Neurosci 18:9620–9628 Available at: http://www.jneurosci.org/content/18/23/9620.full [Accessed August 23, 2015].

Li J, Jiang H, Wong WH (2010) Modeling non-uniformity in short-read rates in RNA-Seq data. Genome Biol 11:R50 Available at: http://www.pubmedcentral.nih.gov/articlerender.fcgi?artid=2898062&tool=pmcentrez&rendertype=abstract [Accessed August 7, 2015].

Li XG, Somogyi P, Ylinen A, Buzsáki G (1994) The hippocampal CA3 network: an in vivo intracellular labeling study. J Comp Neurol 339:181–208 Available at: http://www.ncbi.nlm.nih.gov/pubmed/8300905 [Accessed September 26, 2014].

Lisman JE, Coyle JT, Green RW, Javitt DC, Benes FM, Heckers S, Grace A a (2008) Circuit-based framework for understanding neurotransmitter and risk gene interactions in schizophrenia. Trends Neurosci 31:234–242 Available at: http://www.pubmedcentral.nih.gov/articlerender.fcgi?artid=2680493&tool=pmcentrez&rendertype=abstract [Accessed April 4, 2014].

Logan WJ, Snyder SH (1972) High affinity uptake systems for glycine, glutamic and aspaspartic acids in synaptosomes of rat central nervous tissues. Brain Res 42:413–431 Available at: http://www.ncbi.nlm.nih.gov/pubmed/4340458 [Accessed August 20, 2015].

Luo W, Brouwer C (2013) Pathview: an R/Bioconductor package for pathway-based data integration and visualization. Bioinformatics 29:1830–1831 Available at: http://www.pubmedcentral.nih.gov/articlerender.fcgi?artid=3702256&tool=pmcentrez&rendertype=abstract [Accessed July 30, 2015].

Luo W, Friedman MS, Shedden K, Hankenson KD, Woolf PJ (2009) GAGE: generally applicable gene set enrichment for pathway analysis. BMC Bioinformatics 10:161 Available at: http://www.pubmedcentral.nih.gov/articlerender.fcgi?artid=2696452&tool=pmcentrez&rendertype=abstract [Accessed August 21, 2015].

Lynch MA (2004) Long-term potentiation and memory. Physiol Rev 84:87–136 Available at: http://www.ncbi.nlm.nih.gov/pubmed/14715912 [Accessed December 9, 2014].

Massie A, Goursaud S, Schallier A, Vermoesen K, Meshul CK, Hermans E, Michotte Y (2010) Time-dependent changes in GLT-1 functioning in striatum of hemi-Parkinson rats. Neurochem Int 57:572–578 Available at: http://www.ncbi.nlm.nih.gov/pubmed/20643175 [Accessed August 22, 2015].

McBean GJ (2002) Cerebral cystine uptake: a tale of two transporters. Trends Pharmacol Sci 23:299–302 Available at: http://www.ncbi.nlm.nih.gov/pubmed/12119142 [Accessed August 17, 2015].

Miller BR, Dorner JL, Shou M, Sari Y, Barton SJ, Sengelaub DR, Kennedy RT, Rebec G V (2008) Up-regulation of GLT1 expression increases glutamate uptake and attenuates the Huntington's disease phenotype in the R6/2 mouse. Neuroscience 153:329–337 Available at:

http://www.pubmedcentral.nih.gov/articlerender.fcgi?artid=2424273&tool=pmcentrez&rendertype=abstract [Accessed August 20, 2015].

Mookherjee P, Green PS, Watson GS, Marques MA, Tanaka K, Meeker KD, Meabon JS, Li N, Zhu P, Olson VG, Cook DG (2011) GLT-1 loss accelerates cognitive deficit onset in an Alzheimer's disease animal model. J Alzheimers Dis 26:447–455 Available at: http://www.pubmedcentral.nih.gov/articlerender.fcgi?artid=3256092&tool=pmcentrez&rendertype=abstract [Accessed August 22, 2015].

Ogata H, Goto S, Sato K, Fujibuchi W, Bono H, Kanehisa M (1999) KEGG: Kyoto Encyclopedia of Genes and Genomes. Nucleic Acids Res 27:29–34 Available at: http://www.pubmedcentral.nih.gov/articlerender.fcgi?artid=148090&tool=pmcentrez&rendertype=abstract [Accessed July 15, 2015].

Paula-Lima AC, Brito-Moreira J, Ferreira ST (2013) Deregulation of excitatory neurotransmission underlying synapse failure in Alzheimer's disease. J Neurochem 126:191–202 Available at: http://www.ncbi.nlm.nih.gov/pubmed/23668663 [Accessed March 27, 2014].

Petr G, Sun Y, Frederick N, Zhou Y, Dhamne S, Hameed M, Miranda C, Bedoya E, Fischer K, Armsen W, Wang J, Danbolt N, Aoki C, Rotenberg A, Rosenberg P (2015a) Conditional deletion of the glutamate transporter GLT-1 reveals that astrocytic GLT-1 protects against fatal epilepsy while neuronal GLT-1 contributes significantly to glutamate uptake into synaptosomes. J Neurosci In Press.

Petr GT, Schultheis LA, Hussey KC, Sun Y, Dubinsky JM, Aoki C, Rosenberg PA (2013) Decreased expression of GLT-1 in the R6/2 model of Huntington's disease does not worsen disease progression. Eur J Neurosci 38:2477–2490.

Petr GT, Sun Y, Frederick NM, Zhou Y, Dhamne SC, Hameed MQ, Miranda C, Bedoya EA, Fischer KD, Armsen W, Wang J, Danbolt NC, Rotenberg A, Aoki CJ, Rosenberg PA (2015b) Conditional deletion of the glutamate transporter GLT-1 reveals that astrocytic GLT-1 protects against fatal epilepsy while neuronal GLT-1 contributes significantly to glutamate uptake into synaptosomes. J Neurosci 35:5187–5201 Available at: http://www.ncbi.nlm.nih.gov/pubmed/25834045 [Accessed June 17, 2015].

Prince AM, Andrus L (1992) PCR: how to kill unwanted DNA. Biotechniques 12:358–360 Available at: http://www.ncbi.nlm.nih.gov/pubmed/1571142 [Accessed August 23, 2015].

Przegaliński E, Siwanowicz J, Baran L, Filip M (2000) Activation of serotonin (5-HT)1A receptors inhibits amphetamine sensitization in mice. Life Sci 66:1011–1019 Available at: http://www.ncbi.nlm.nih.gov/pubmed/10724448 [Accessed August 23, 2015].

Rempe D, Vangeison G, Hamilton J, Li Y, Jepson M, Federoff HJ (2006) Synapsin I Cre transgene expression in male mice produces germline recombination in progeny. Genesis 44:44–49 Available at: http://www.ncbi.nlm.nih.gov/pubmed/16419044 [Accessed April 18, 2014].

Robbins TW, Everitt BJ (1996) Neurobehavioural mechanisms of reward and motivation. Curr Opin Neurobiol 6:228–236 Available at: http://www.ncbi.nlm.nih.gov/pubmed/8725965 [Accessed August 23, 2015].

Roberts A, Pimentel H, Trapnell C, Pachter L (2011a) Identification of novel transcripts in annotated genomes using RNA-Seq. Bioinformatics 27:2325–2329 Available at: http://bioinformatics.oxfordjournals.org/content/27/17/2325 [Accessed July 14, 2014].

Roberts A, Trapnell C, Donaghey J, Rinn JL, Pachter L (2011b) Improving RNA-Seq expression estimates by correcting for fragment bias. Genome Biol 12:R22 Available at: http://genomebiology.com/2011/12/3/R22 [Accessed July 10, 2014].

Rose EM, Koo JCP, Antflick JE, Ahmed SM, Angers S, Hampson DR (2009) Glutamate transporter coupling to Na,K-ATPase. J Neurosci 29:8143–8155 Available at: http://www.ncbi.nlm.nih.gov/pubmed/19553454 [Accessed August 23, 2015].

Rothstein JD, Martin L, Levey AI, Dykes-Hoberg M, Jin L, Wu D, Nash N, Kuncl RW (1994) Localization of neuronal and glial glutamate transporters. Neuron 13:713–725 Available at: http://www.ncbi.nlm.nih.gov/pubmed/7917301 [Accessed April 18, 2014].

Schulz TJ, Glaubitz M, Kuhlow D, Thierbach R, Birringer M, Steinberg P, Pfeiffer AFH, Ristow M (2007) Variable expression of Cre recombinase transgenes precludes reliable prediction of tissue-specific gene disruption by tail-biopsy genotyping. PLoS One 2:e1013 Available at: http://www.pubmedcentral.nih.gov/articlerender.fcgi?artid=1995755&tool=pmcentrez&rendertype=abstract [Accessed August 23, 2015].

Shoffner JM (1997) Oxidative phosphorylation defects and Alzheimer's disease. Neurogenetics 1:13–19 Available at: http://www.ncbi.nlm.nih.gov/pubmed/10735269 [Accessed August 23, 2015].

Small SA, Schobel SA, Buxton RB, Witter MP, Barnes CA (2011) A pathophysiological framework of hippocampal dysfunction in ageing and disease. Nat Rev Neurosci 12:585–601 Available at: http://www.pubmedcentral.nih.gov/articlerender.fcgi?artid=3312472&tool=pmcentrez&rendertype=abstract [Accessed July 31, 2015].

Smeitink J, van den Heuvel L, DiMauro S (2001) The genetics and pathology of oxidative phosphorylation. Nat Rev Genet 2:342–352 Available at: http://www.ncbi.nlm.nih.gov/pubmed/11331900 [Accessed August 23, 2015].

Takahashi M, Billups B, Rossi D, Sarantis M, Hamann M, Attwell D (1997) The role of glutamate transporters in glutamate homeostasis in the brain. J Exp Biol 200:401–409 Available at: http://www.ncbi.nlm.nih.gov/pubmed/9050249 [Accessed August 20, 2015].

Tanaka K, Watase K, Manabe T, Yamada K, Watanabe M, Takahashi K, Iwama H, Nishikawa T, Ichihara N, Kikuchi T, Okuyama S, Kawashima N, Hori S, Takimoto M, Wada K (1997) Epilepsy and exacerbation of brain injury in mice lacking the glutamate transporter GLT-1. Science 276:1699–1702 Available at: http://www.ncbi.nlm.nih.gov/pubmed/9180080 [Accessed March 28, 2014].

Thiemann G, Di Marzo V, Molleman A, Hasenöhrl RU (2008) The CB(1) cannabinoid receptor antagonist AM251 attenuates amphetamine-induced behavioural sensitization while causing monoamine changes in nucleus accumbens and hippocampus. Pharmacol Biochem Behav 89:384–391 Available at: http://www.ncbi.nlm.nih.gov/pubmed/18294680 [Accessed August 23, 2015].

Trapnell C, Hendrickson DG, Sauvageau M, Goff L, Rinn JL, Pachter L (2013) Differential analysis of gene regulation at transcript resolution with RNA-seq. Nat Biotechnol 31:46–53 Available at: http://dx.doi.org/10.1038/nbt.2450 [Accessed July 9, 2014].

Trapnell C, Pachter L, Salzberg SL (2009) TopHat: discovering splice junctions with RNA-Seq. Bioinformatics 25:1105–1111 Available at: http://bioinformatics.oxfordjournals.org/content/25/9/1105.abstract [Accessed July 10, 2014].

Trapnell C, Roberts A, Goff L, Pertea G, Kim D, Kelley DR, Pimentel H, Salzberg SL, Rinn JL, Pachter L (2012) Differential gene and transcript expression analysis of RNA-seq experiments with TopHat and Cufflinks. Nat Protoc 7:562–578 Available at: http://www.pubmedcentral.nih.gov/articlerender.fcgi?artid=3334321&tool=pmcentrez&rendertype=abstract [Accessed July 9, 2014].

Trapnell C, Williams BA, Pertea G, Mortazavi A, Kwan G, van Baren MJ, Salzberg SL, Wold BJ, Pachter L (2010) Transcript assembly and quantification by RNA-Seq reveals unannotated transcripts and isoform switching during cell differentiation. Nat Biotechnol 28:511–515 Available at: http://dx.doi.org/10.1038/nbt.1621 [Accessed July 9, 2014].

Wang XH, Lu G, Hu X, Tsang KS, Kwong WH, Wu FX, Meng HW, Jiang S, Liu SW, Ng HK, Poon WS (2012) Quantitative assessment of gait and neurochemical correlation in a classical murine model of Parkinson's disease. BMC Neurosci 13:142 Available at: http://www.pubmedcentral.nih.gov/articlerender.fcgi?artid=3507899&tool=pmcentrez&rendertype=abstract [Accessed August 23, 2015].

Wilson CJ (1987) Morphology and synaptic connections of crossed corticostriatal neurons in the rat. J Comp Neurol 263:567–580 Available at: http://www.ncbi.nlm.nih.gov/pubmed/2822779 [Accessed August 23, 2015].

Wolf ME (1998) The role of excitatory amino acids in behavioral sensitization to psychomotor stimulants. Prog Neurobiol 54:679–720 Available at: http://www.ncbi.nlm.nih.gov/pubmed/9560846 [Accessed August 23, 2015].

Yano S, Tokumitsu H, Soderling TR (1998) Calcium promotes cell survival through CaM-K kinase activation of the protein-kinase-B pathway. Nature 396:584–587 Available at: http://www.ncbi.nlm.nih.gov/pubmed/9859994 [Accessed August 20, 2015].

Yogev G, Plotnik M, Peretz C, Giladi N, Hausdorff JM (2007) Gait asymmetry in patients with Parkinson's disease and elderly fallers: when does the bilateral coordination of gait require attention? Exp brain Res 177:336–346 Available at: http://www.ncbi.nlm.nih.gov/pubmed/16972073 [Accessed August 23, 2015].

Zink M, Vollmayr B, Gebicke-Haerter PJ, Henn FA (2010) Reduced expression of glutamate transporters vGluT1, EAAT2 and EAAT4 in learned helpless rats, an animal model of depression. Neuropharmacology 58:465–473 Available at: http://www.ncbi.nlm.nih.gov/pubmed/19747495 [Accessed August 20, 2015].